TAL TECH

TALLINN UNIVERSITY OF TECHNOLOGY
SCHOOL OF ENGINEERING
Department of Electrical Power Engineering and Mechatronics

HIGH-PERFORMANCE MECHATRONICS DESIGN FOR SCANNING DROPLET ADHESION MICROSCOPE

KÕRGJÕUDLUSEGA MEHHATROONIKA DISAIN TILKADE HAARDETEGURI MIKROSKOOBI SKANEERIMISEKS

MASTER THESIS

Student:	Seyed Shahriar Najafi Haeri
Student code:	177185 MAHM
Supervisors:	Quan Zhou, Associate professor
	Mart Tamre, Professor

Tallinn 2020

AUTHOR'S DECLARATION

Hereby I declare, that I have written this thesis independently.

No academic degree has been applied for based on this material. All works, major viewpoints and data of the other authors used in this thesis have been referenced.

"20" 12. / .... 2019.....

Author:.......... _Al Haeri_

/signature /

Thesis is in accordance with terms and requirements

"20" 12 2019....

Supervisor: ....

/signature/

Accepted for defence

" " ....2020....

Chairman of theses defence commission: ....

/name and signature/

Non-exclusive Licence for Publication and Reproduction of GraduationTthesis[1]

I, Seyed Shahriar Najafi Haeri (date of birth: 31.07.1992) hereby

1. grant Tallinn University of Technology (TalTech) a non-exclusive license for my thesis High-performance Mechatronics Design for Scanning Droplet Adhesion Microscope,

supervised by Professor Quan Zhou and Professor Mart Tamre.

1.1 reproduced for the purposes of preservation and electronic publication, incl. to be entered in the digital collection of TalTech library until expiry of the term of copyright;

1.2 published via the web of TalTech, incl. to be entered in the digital collection of TalTech library until expiry of the term of copyright.

1.3 I am aware that the author also retains the rights specified in clause 1 of this license.

2. I confirm that granting the non-exclusive license does not infringe third persons' intellectual property rights, the rights arising from the Personal Data Protection Act or rights arising from other legislation.

---

[1] *Non-exclusive Licence for Publication and Reproduction of Graduation Thesis is not valid during the validity period of restriction on access, except the university`s right to reproduce the thesis only for preservation purposes.*

_____ (signature)

3.1.2020 (date)

3

THESIS TASK

Student: Seyed Shahriar Najafi Haeri, 177185MAHM (name, student code)

Study programme, MAHM02/13 - Mechatronics (code and title)

main specialty: Mechatronics

Supervisor(s): Associate Professor, Quan Zhou, +358408550311 (position, name, phone)

Professor, Mart Tamre, +3725120982 (position, name, phone)

Consultants: ....(name, position)

.... (company, phone, e-mail)

Thesis topic:

(in English)   _High-performance mechatronics design for scanning droplet adhesion microscope_

(in Estonian)   _Suure jõudlusega seade tilkade skaneerimiseks adhesioonimikroskoobil_ ''

Thesis main objectives:

1. Mechatronics design and implementation for SDAM

2. Performance analysis for new design

3. Instrument development based on user feedback

Thesis tasks and time schedule:

No	Task description	Deadline
1.	Mechatronics design and implementation	30.03.2019
2.	Performance analysis for new design	31.07.2019
3.	Instrument development	30.11.2019

Language: English   **Deadline for submission of thesis:** "03" January 2020....a

Student: Shahriar Najafi Heri .... _[signature]_ .... "20" 12 ....2019....a

/signature/

Supervisor: Quan Zhou .... _[signature]_ .... "20" 12 ....2019....a

/signature/

Supervisor: Mart Tamre .... "......"......................2020....a

/ signature /

Terms of thesis closed defence and/or restricted access conditions to be formulated on the reverse side

Contents

PREFACE

Seyed Shahriar Najafi Haeri
Espoo, January 2020

LIST OF ABBREVIATIONS AND SYMBOLS

2D   Two dimensional

3D   Three dimensional

AFM   Atomic force microscopy

CCD   Charge-coupled device camera

DOF   Degree of Freedom

FOV   Field of View

GUI   Graphical User Interface

MEMS   Micro-electro-mechanical systems

SDAM   Scanning droplet adhesion microscopy

SPM   Scanning probe microscopy

UI   User interface

UX   User experience

α Sliding angle, °

γ Surface tension of water, $J.m^{-2}$ or $N.m^{-1}$

γ_{LG} Liquid-gas interfacial tension, $J.m^{-2}$

γ_{SG} Solid–gas interfacial tension, $J.m^{-2}$

γ_{SL} Solid-liquid interfacial tension, $J.m^{-2}$

θ_A Advancing contact angle, °

θ_R Receding contact angle, °

θ_Y Young's contact angle, °

θ^* Apparent contact angle, °

$\Delta\rho$ Difference in density, $g.cm^{-3}$

ε_0 Dielectric permittivity, $F.m^{-1}$

A	Active capacitive area, m^2
C	Capacitance, Farad
d	Distance between plates, m
g	Acceleration due to gravity, $m.s^{-2}$
H	Contact angle hysteresis, °
V	Volume, m^3
V_0	Output voltage, volt
V_s	Supply voltage, volt
W	Work of adhesion, $J.m^{-2}$

1. INTRODUCTION

Wetting is the study of contact between the liquid and solid surface. The wetting phenomenon manifests in nature through directional wetting of rice leaf, self-cleaning of lotus leaf, and reflectivity of a butterfly wing. The wettability of these biological surfaces inspires scientists to synthesize water repellent surfaces with outstanding wetting properties.

Very water-repelling surfaces, also known as superhydrophobic surfaces, will not be wetted by water, which enables many outstanding properties such as self-cleaning [1], anti-fogging [2], anti-icing [3], anti-corrosion [4], etc. Although a wealth of research has done on mechanisms of wetting, starting from the groundbreaking work of Wenzel [5] and Cassie and Baxter [6], it is still one of the hot topics in the research field. A better understanding of the superhydrophobic phenomenon [7] can not only advance the fabrication of bio-inspired surfaces but also boost their applications both in biology and technology [8]–[11]. Self-cleaning fabrics, eyeglasses, car windscreens, and mirrors are just a few examples of superhydrophobic bioinspired surfaces, which have already found their applications.

Optical contact angle measurement is a widely used method for wetting characterization, where the contact angle between the sessile droplet and solid surface measured. The contact angle indicates the extent of wetting when a solid and liquid interacts. Contact angles less than 90° corresponds to high wettability, and contact angle larger than 90° indicates low wettability. Due to the high contact angle in superhydrophobic surfaces, the optical method will fail to reliably indicate the baseline and estimate the contact angle with high accuracy and repeatability. Besides, superhydrophobic surfaces often contain microscopic irregularities in surface texture and composition, which may affect or even govern macroscopic wetting phenomena [12]. Typically, the contact angle is measured and announced for a single point to represent the entire surface wettability, which does not reveal surface inhomogeneity and local wetting variations.

Wetting characterization can also be done by measuring the normal and in-plane contact forces of droplets on the surface [13][14]. Force-based methods, including force tensiometry, directly measure adhesion forces during the contact and separation process between the droplet and a solid surface. Hanging the droplet from a ring attached to a stationary micro-force sensor, and approaching the sample towards it will result in establishing contact between water droplet and surface, which corresponds to

in-plane force, also known as snap-in force. Gradual retraction of droplet and sample will lead to separation of solid surface and droplet, which is known as normal adhesion force or pull-off force. Although snap-in and pull-off forces can reveal surface homogeneity and wetting characteristics, the prevalent force tensiometry is not sensitive enough to detect small forces for superhydrophobic surfaces, especially in case of the snap-in force.

Highly accurate and precise methods for a comprehensive understanding of the wetting mechanism on superhydrophobic surfaces can broaden the horizons in this field. The scanning droplet adhesion microscopy (SDAM) is a novel technique for wetting characterization with three orders of magnitude better force sensitivity than current force tensiometers and spatial resolution down to 10 μm [12]. Scanning the sample surface with extremely high force sensitivity is aided by liquid droplet micro-force sensing probe and precise motorized positioners, which allows detection of minor spatial differences on flat and non-flat surfaces.

The SDAM is the result of a collaborative research effort of the Robotic Instrument research group and Soft Matter and Wetting research group at Aalto University. Although the SDAM technique is a scientifically groundbreaking work, the measurement instrument needs further developments in performance and usability to empower scientists in academy and industry for wetting characterization of samples in a great deal.

The early-stage proof-of-concept suffers from issues such as low performance and time-consuming preparation procedures. Besides, the ad hoc construction of the set-up is hard to improve, and systematic design and implementation are necessary. The objective of this thesis work is to address these limitations in early-stage design for scanning droplet adhesion microscope. High-performance design can be interpreted as a robust microscope with high accuracy and repeatability that benefits from simple preparation procedure and high scanning speed. Also, the new design should provide flexibility for continuous developments.

Mentioned objectives of this thesis work can be summarized in the following research questions:
1. What are the most critical mechatronic limitations in early-stage SDAM?
2. How may the new design address the limitations to achieve high-performance SDAM?

The thesis consists of six chapters. The current chapter (introduction) describes

motivations for conducting research on SDAM, introduces desired objectives, and research questions. Chapter 2 reviews the fundamentals of wetting and state-of-the-art techniques for wetting characterization, including scanning droplet adhesion microscopy. Chapter 3 provides an overview of early-stage SDAM mechatronics design, the most critical mechatronics aspects, and limitations. In chapter 4, the requirements for high-performance SDAM discussed, and the contribution of the author described by reviewing the design process of a new instrument. Chapter 5 evaluates the system performance for new SDAM and expresses the ideas for future improvements. In summary, the overview of the process, results, and future works are expressed.

2. WETTING MEASUREMENT TECHNOLOGY

Wetting has attracted a lot of interest from the fundamental and industrial point of view. Surface wetting characteristics play a crucial role in industrial processes, such as coating, painting, printing, de-icing, etc. There is an increasing interest in superhydrophobic surfaces due to their exceptional wetting properties, which enabling remarkable functions in technology and biology [12], [15]–[19].

This chapter highlights the fundamentals of the wetting concept, and techniques that are commonly used to characterize solid surface wettability, including optical method and force-based methods. A novel technique for superhydrophobic wetting characterization called scanning droplet adhesion microscopy is described. This technique enables scientists to obtain wetting maps with three orders of magnitude better force sensitivity than current force tensiometers with a spatial resolution down to 10 µm [12], [19], [20].

Pros and cons of state-of-the-art techniques for wetting characteristics of water-repellent surfaces presented, and the conclusion is drawn to clarify the motivation for researching this topic.

2.1 Surface tension and contact angle-Young's Equation

Considering a homogeneous liquid, molecules in the bulk of liquid pulling to different directions with the same forces applied by neighboring molecules, resulting in a net force of zero. However, the molecules exposed to the surface get more attractive forces towards the bulk of liquid molecules. Since air-liquid adhesive forces are much less than liquid-liquid force, molecules exposed to the surface pulled inward by neighboring molecules in a liquid. This intermolecular force to contract the surface is called the surface tension is shown in Figure 2.1. The surface tension is also responsible for the shape of liquid droplets [7], [19], [20].
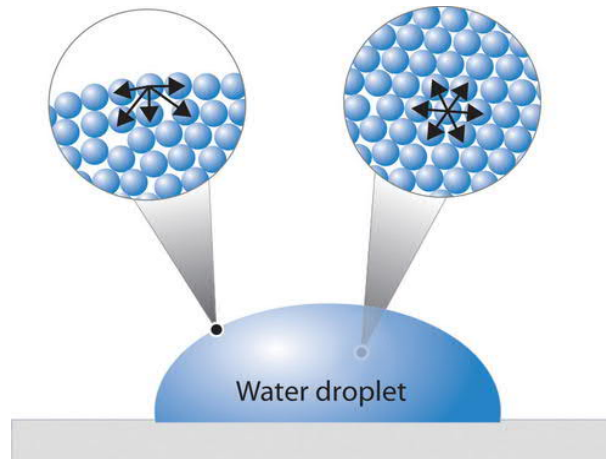
Figure 2.1 Illustration of surface tension:
Molecules exposed to surface experience fewer interactions compared to the molecules inside the bulk, resulting in excess energy at the surface [7].

Wetting is the study of how a liquid deposited on a solid surface spreads. The area of interest is where the three phases (liquid, solid, gas) contact each other, known as triple line, or contact line. Contact line geometrically acquired by applying a tangent line from the contact point along with the liquid-gas interface in the droplet profile, shown in Figure 2.2.
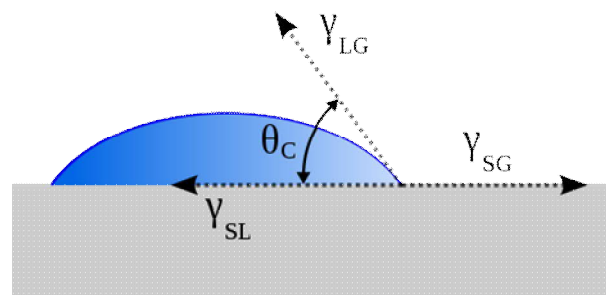
Figure 2.2 Illustration of contact angle and interfacial tensions [7].

As first described by Thomas Young in 1805, the contact angle of a liquid drop on an ideal solid surface defined by the mechanical equilibrium of the droplet under the action of three interfacial tensions. Equation (2.1) usually referred to Young's equation, and θ_Y is (Young's) contact angle [7].

$$\gamma_{LG} \cos \theta_Y \ = \ \gamma_{SG} \ - \ \gamma_{SL} \tag{2.1}$$

Where γ_{LG} , γ_{SG} , and γ_{SL} represent the liquid-gas, solid-gas, and solid-liquid interfacial

tensions, respectively. For instance, complete wetting occurs when the contact angle is 0°, as the droplet turns into a flat puddle. Solids with high surface energy, such as glass and silicon, are readily wetted by liquids since it is more favorable for liquid with low surface energy to cover surfaces with high energy [7][20].

On the other hand, surfaces with contact angle more than 150°, known as superhydrophobic, have low surface energy, and they are not wetted by liquid easily. In this case, energy minimization leads to higher contact angle with a smaller contact area since the liquid surface tension is considerably higher than solid surface tension. Different contact angles are shown in Figure 2.3.
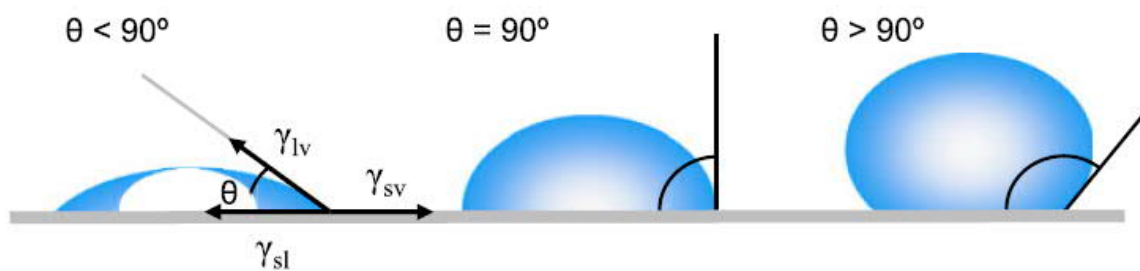

Figure 2.3 Illustration of different contact angles formed by sessile liquid drops on different solid surfaces:
Contact angle less than 90° categorized in hydrophilic and more than 90° hydrophobic surfaces [7].

The contact angle defined by Young's Equation (2.1) referred to the ideal contact angle (θ_Y), and it is valid only for perfect solids whose surfaces are homogeneous, isotropic, smooth, and rigid when surrounding fluids are inert to such a solid (no chemical reaction or specific adsorption, dissolution, swelling, or rearrangement of phases, molecules, and functional groups) [21]–[23]. However, due to surface roughness in the contact line, the measured contact angle and Young's contact angle described by Wenzel's model represented in Equation (2.2) [7].

$cos\ \theta^* =\ r\ cos\ \theta_Y$ (2.2)

Where r is the roughness factor, i.e., the ratio of the actual surface area in contact with the liquid to the apparent, projected wetted area. Apparent contact angle θ^* is lower than Young's contact angle if $\theta_Y < 90°$ and apparent contact angle will be higher if $\theta_Y > 90°$. Therefore, surface roughness can improve wettability in hydrophilic surfaces.

15

2.2 Optical tensiometer

Direct contact angle measurement is a widely used technique, which tangent angle at the three-phase contact point on a sessile drop profile measured by an optical tensiometer.

An optical tensiometer or contact angle goniometer is a simple instrument. The first commercial contact angle goniometer was designed by W.A. Zisman, and manufactured by ramé-hart instrument company in the early 1960s, as shown in Figure 2.4.

Figure 2.4 A ramé-hart contact angle goniometer:
The first commercial contact angle goniometer, designed by W.A. Zisman, manufactured by ramé [7].

Contact angle goniometers instrument consists of a sample holder stage, a dispensing module to form a liquid drop in µl order on the surface, a camera equipped with a microscope objective, and backlight illumination. In current versions of contact angle goniometer, the measurement is done by machine vision algorithms that measure the tangent of the sessile drop profile at the contact point with the surface and provide estimation for contact angle.

Over the decades, the instrument hardware as well as contact angle algorithms, and user interface have developed to improve the instrument performance. Motor-Driven dispensers are widely used to control the rate of liquid addition and removal to study advancing, receding, or dynamic contact angles [7]. Manual and automated sample

stages enable the user to measure contact angle for different points of sample surfaces. Multi-dispenser versions can accelerate the measurement time whenever the contact angle for different liquids are essential to the measurement. A multi-dispenser goniometer and its GUI manufactured by DataPhysics company shown in Figure 2.5. The Instrument comprises a manual sample stage, multi-dispensers, a microscope camera, and backlight.

Figure 2.5 OCA 25 contact angle goniometer manufactured by DataPhysics, GmbH, Germany [24].

2.2.1 Dynamic contact angle and hysteresis

As discussed in section 2.1, Young's Equation (2.1), known as static contact angle assumes smooth, homogeneous, isotropic, and rigid surfaces, which does not exist in reality. Due to the physical or chemical heterogeneity of real surfaces, the wetting phenomenon is a dynamic state. Therefore, the static contact angle cannot be used to predict precisely the equilibrium contact angle on real surfaces. In practice, liquid moves to expose to the fresh surface, and the contact area of a solid-liquid is not symmetric. That is one of the reasons, which observed contact angles are not equal to Young's contact angle θ_Y.

Advancing and receding contact angles, referred as dynamic contact angle, occurs in the course of wetting (advancing angle) and de-wetting (receding angle) of a solid when a three-phase contact line is in actual motion. The advancing contact angle θ_A formed

17

by expanding liquid, occurs on the wetting phase, is higher than the receding contact angle θ_R, which occurs by contracting the liquid on the surface [25].

The rate of adding or absorbing liquid must not be too great to avoid falsifying the measurement by the introduction of mechanical energy. On the other hand, it must not be too slow to rule out the time effects.

Advancing and receding contact angle can also be observed when a droplet pinned on a tilted solid surface. If the tilt angle (α) is less than the critical angle, the droplet will not move or slide on the surface but rather deforms as illustrated in Figure 2.6a. Droplet's shape is defined by the balance between gravity force and the solid surface tension, as illustrated in Figure 2.6b [19][25].
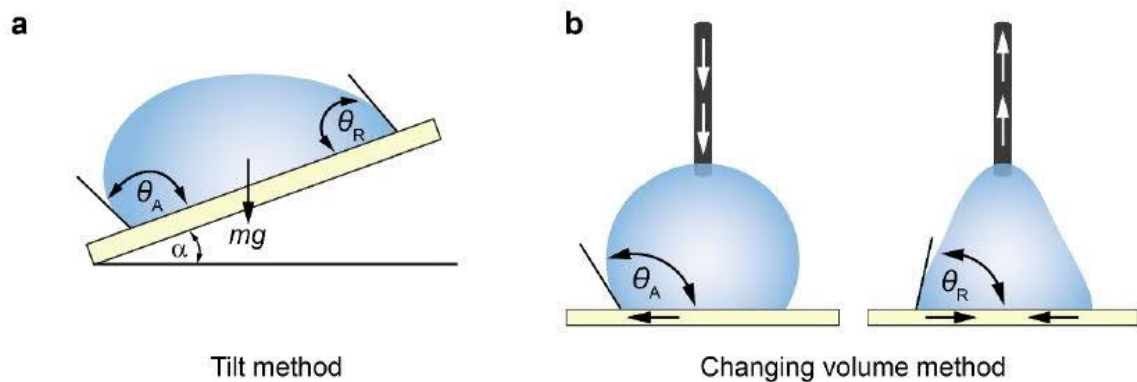

Figure 2.6 Illustration of advancing and receding contact angles:
(a) Determination of the advancing, θ_A, and receding, θ_R, contact angle by tilt method. (b) Determination of the advancing, θ_A, and receding, θ_R, contact angle by tilt method [19].

The difference between the advancing contact angle and the receding contact angle so-called contact angle hysteresis (H) [26].

$$H = \theta_A - \theta_R \tag{2.3}$$

The contact angle goniometer is a simple instrument, which works based on the fundamentals of wetting in a semi-automated manner. The measurement is recorded as a video file, and then by machine vision algorithms, the contact angle can be calculated and exported for data processing. The same instrument can perform a variety of measurements such as surface and interfacial tension measurements (pendant droplet method), static and dynamic contact angle measurement (contact angle hysteresis), liquid bridge analysis, etc.

On the other hand, for accuracy and reproducibility of the indirect optical method, baseline detection and assigning exact tangent line are essential. Misalignment can cause a significant error and inconsistency of the results obtained by different users [12][27][28]. The optical methods can give accurate results for hydrophilic/phobic surfaces (e.g., ± 0.1°, but this technique provides less accurate results for superhydrophobic surfaces) [29][30]. The accuracy of optical measurements for sessile drops on liquid-repellent surfaces decreases as the contact angle approaches to 180°. An uncertainty as small as 1 μm in the location of the droplet baseline or droplet height can result in an uncertainty in the contact angle as large as 10° [31]. Variations of the contact point along the three-phase contact line could happen due to surface heterogeneity or roughness. Despite all of these issues, the goniometer method is considered as the most convenient method if high accuracy is not required for hydrophilic/phobic surfaces [7].

2.3 Force tensiometer

Force tensiometer is a device mainly used for measuring the surface tension of a liquid and the interfacial tension between two liquids. Also, some techniques can measure solid surface tension and indirectly calculate contact angles, such as the Wilhelmy plate and ring method. The Wilhelmy plate method initially implemented for liquid surface tension where the used plate is made out of iridium–platinum to have a good wetting property ($\theta_Y = 0$). Later, this method has adapted, and various practices have done to measure dynamic contact angle. In these practices, instead of iridium–platinum plate, a solid sample plate is hanging from a microbalance immersed and retracted from a reservoir filled with a liquid with known surface tension. Force tensiometer and Wilhelmy plate method used for liquid surface tension measurement are shown in Figure 2.7.
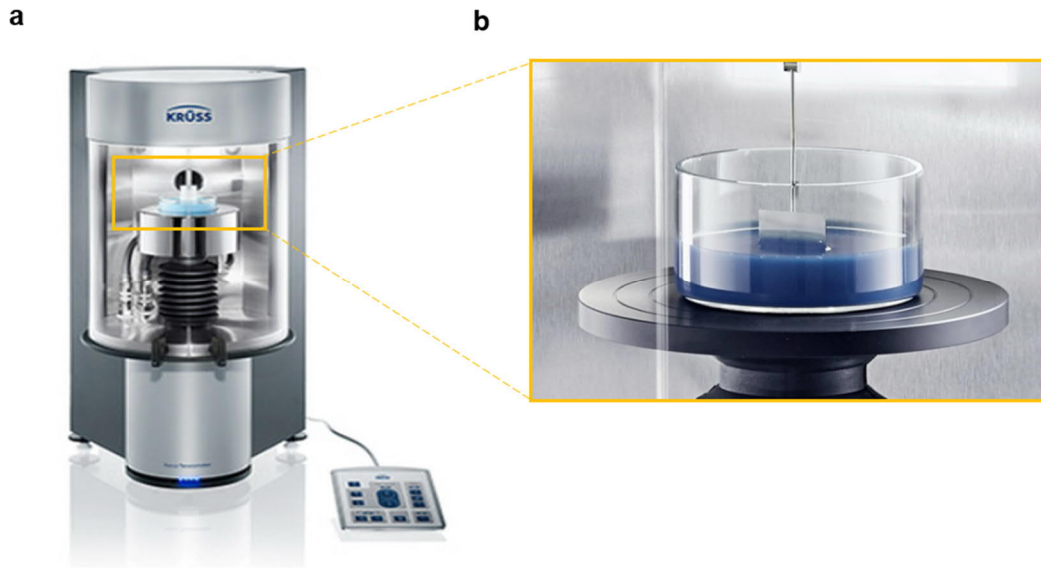
Figure 2.7 Force tensiometer manufactured by KRUSS Company, GmbH, Germany [32]: (a) The device comprises a microbalance and a sample holder, which moves the sample vertically. (b) The typical Wilhelmy plate attached to microbalance while the sample stage is going down with a steady speed (receding cycle).

2.3.1 Wilhelmy plate method

Wilhelmy plate method is categorized as a force-based method for indirect dynamic contact angle measurement on a solid surface. When a thin, smooth, vertical sample plate brought in contact with a liquid, the change in detected forces value is recorded by a microbalance and plotted versus depth of immersion. The detected force change comprises of wetting force, buoyancy, and solid sample weight. The wetting force f can be calculated as defined in Equation (2.4) [7].

$$f = \gamma_{lv}\, p \cos\theta \tag{2.4}$$

Where γ_{lv} is the liquid surface tension, p is the perimeter of the contact line (i.e., the same as the perimeter of solid sample's cross-section), and θ is the contact angle. Consequently, the total detected force change, F_{total}, is as follow:

$$F_{total} = \gamma_{lv}\, p \cos\theta - V\Delta\rho g + W \tag{2.5}$$

In Equation (2.5), the first term represents the wetting force, the second term represents the buoyancy force, and the third term represents the weight of the sample. Where V is the volume of the displaced liquid, $\Delta\rho$ is the difference in density between the liquid and air (or a second liquid), g is the acceleration of gravity, and W is the weight of the sample and hanging rod.
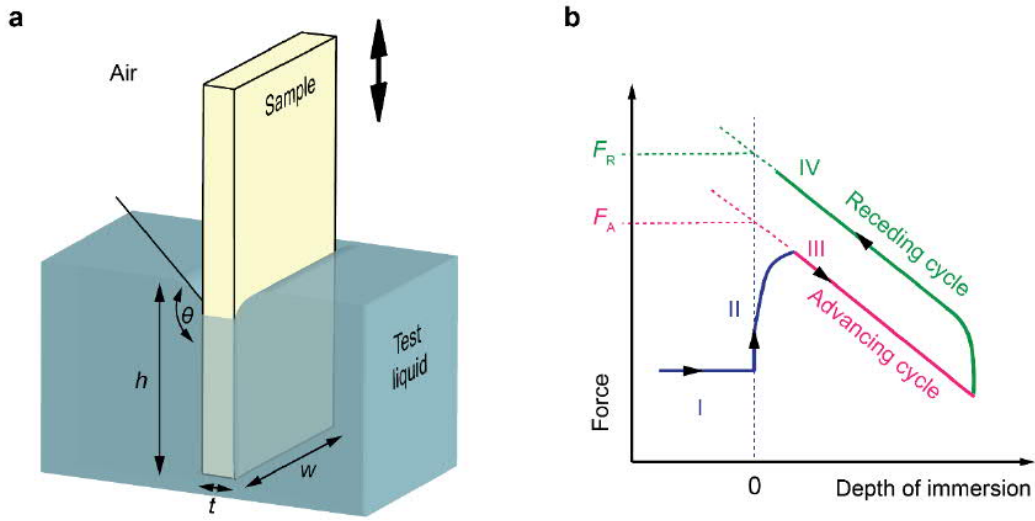
Figure 2.8 The Wilhelmy plate method concept implemented for contact angles measurement: (a) Schematic illustration shows immersion of the sample in the liquid with known surface tension where w denotes sample width, t denotes sample thickness, and h denotes immersion depth. (b) The typical force curve depicting four steps were (I) corresponds to the solid sample before contact with liquid surface, (II) the first contact between solid and liquid sample, (III) corresponds to immersion of sample plate up to certain depth (represent advancing angle), and (IV) corresponds to the retraction of the sample (represent receding angle), and force values recorded during immersion process (advancing cycle), F_A, and retraction process (receding cycle), F_R [19].

During the immersion, the liquid advances on the sample. The total force applied to the sample in advancing cycle is less due to the buoyancy force. The wetting force can be calculated by linear regression of recorded weight and extrapolation to zero-depth immersion for obtaining buoyancy corrected wetting force for advancing cycle, F_A.

While the liquid surface tension, the solid perimeter, and plate weight are known, the dynamic contact angle value can be calculated by Equation (2.6 and 2.7) [7].

$$cos\ \theta_A = \frac{F_A}{\gamma_{lv}} \tag{2.6}$$

In the next cycle, the sample is pulled out, and the liquid is receding from the sample, marked as IV in Figure 2.8. The buoyancy corrected wetting force is calculated the same way as advancing contact angle. The receding contact angle can be calculated as described in Equation (2.7) [7].

$$cos\ \theta_R = \frac{F_R}{\gamma_{lv}} \tag{2.7}$$

21

For calculating the dynamic contact angle using the Wilhelmy plate method, wetted length (perimeter) should be known to us. Due to surface roughness, finding accurate wetted length is challenging for superhydrophobic surfaces, and it can lead to an inaccurate evaluation of contact angle [33].

2.3.2 Adhesion force tensiometry

Another approach to characterize the wettability of the surface is obtaining adhesive properties. Adhesion forces can provide a better understanding of wetting, especially for studying surface inhomogeneity. These normal forces can be measured directly via the process in which the hanging droplet attached to the force sensor or microbalance with high resolution. The sample is approaching the droplet, and the first contact between them is known as snap-in force (marked as B in Figure 2.9a). Once the contact is established, the capillary force starts to act between the liquid droplet and the surface. In the next cycle, the hydrophobic surface is gradually retracting. The recorded force when the droplet is detaching from the hydrophobic surface is known as pull-off force (marked as E in Figure 2.9a). Accordingly, the snap-in force can be correlated with the work of adhesion for advancing, W_A, and the advancing contact angle, θ_A. Similarly, the pull-off force can be correlated with the work of adhesion for receding/separation, W_R, and the receding contact angle, θ_R [3].
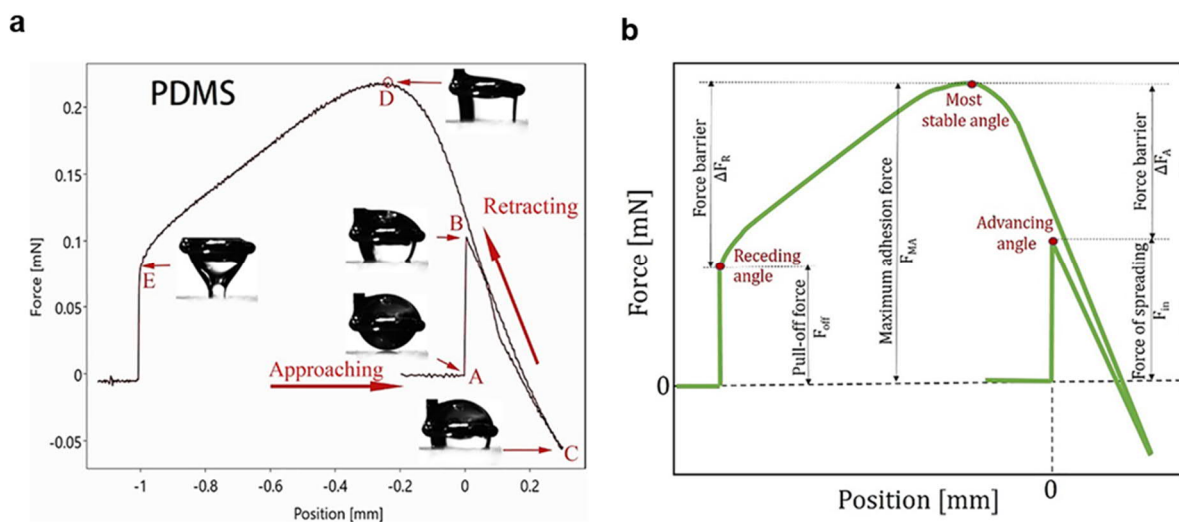

Figure 2.9 Force curve generated by PDMS force tensiometry and its correlation with marked key parameters:
(a) Full-cycle snapshots when the sample is approaching towards the droplet. (A) solid surface approach to droplet, before contact, (B) snap-in force when sample is in contact with the liquid, (C) continuous movement towards the droplet, (D) retraction of sample and droplet (detection of maximum force), (E) pull-off force when separation of sample and droplet has happened. (b) Correlation of snap-in and pull-off forces with advancing and receding contact angles [23].

Once the contact established, the further movement towards droplet (marked as C in Figure 2.9a) is identical to advancing the droplet on the surface and retraction of surface and droplet (marked as E in Figure 2.9a) recedes contact line. The corresponding force events are related to advancing θ_A, and receding contact angle θ_R, respectively [12][34]. The work of adhesion per unit area applied to de-wet the surface can be expressed by Dupré's Equation (2.8) [34].

$$W = \gamma_{SG} - \gamma_{SL} + \gamma \tag{2.8}$$

By considering Young's Equation (2.1), the Dupré's Equation (2.8) can be rewritten as Equation (2.9) [34]:

$$W = \gamma(1 + cos\ \theta) \tag{2.9}$$

Force tensiometry has several advantages over conventional optical methods. First, the task of locating an accurate baseline and finding the corresponding contact angle is reduced to the weight and length measurement that can be performed by the user with high accuracy. Second, the measured force at any given depth of immersion is an averaged value that provides more accurate contact angle value. The obtained contact angle reflects the wetting property of the entire sample. Besides, the force curve obtained by force tensiometer (Figure 2.8) can reveal dynamic contact angles as well as contact angle hysteresis at different wetting and dewetting speeds. The smoothness of the plotted force curve indicates solid surface heterogeneity. However, the Wilhelmy method is prone to some errors. The solid sample cross-section in the submersion plate needs to be prepared with uniform edges. Ideally, rods, plates, and fibers sample perimeters are known. It is sometimes challenging to find the wetted length and to assign exact perimeters. Other than optical goniometer, the solid sample must have the same characteristics and topography at entire dimensions that are difficult to reach, especially if biological samples are subject of measurement.

On the other hand, adhesion force tensiometry is potentially attractive since the measurement sample area is limited to the three-phase contact area. This method can provide surface inhomogeneity and local variation of wetting properties [12][23]. Unfortunately, the force tensiometry method is not sensitive enough to detect small forces between the water droplet and superhydrophobic surfaces (maximum resolution down to μN). Also, this method suffers from low spatial resolution due to the big droplet size.

2.4 Scanning Droplet Adhesion Microscope (SDAM)

The scanning droplet adhesion microscope illustrated in Figure 2.10. The instrument comprises of a stationary force sensor with a liquid droplet probe (e.g., water) attached to the sensor tip. The force sensing probe mounted vertically. Multi-axis sample stages for moving the solid sample are used. The measuring adhesion forces are possible point-by-point in a fully automated manner with a high resolution and repeatability. Measurements are monitored from two sides using one high-speed camera, and one CCD camera mounted perpendicular to the force sensing probe, to make sure the force sensing probe is aligned. The measurement steps can be recorded for data analysis.

A micro-dispenser with a piezoelectric actuator is used for dispensing sub-microliter droplets. The dispenser should be aligned with the force sensing probe in a way that the dispensed droplets bounce off a superhydrophobic surface and form a big droplet attached to SU-8 disk. The instrument set-up is installed on a vibration isolation table since it is sensitive to vibration and noise.
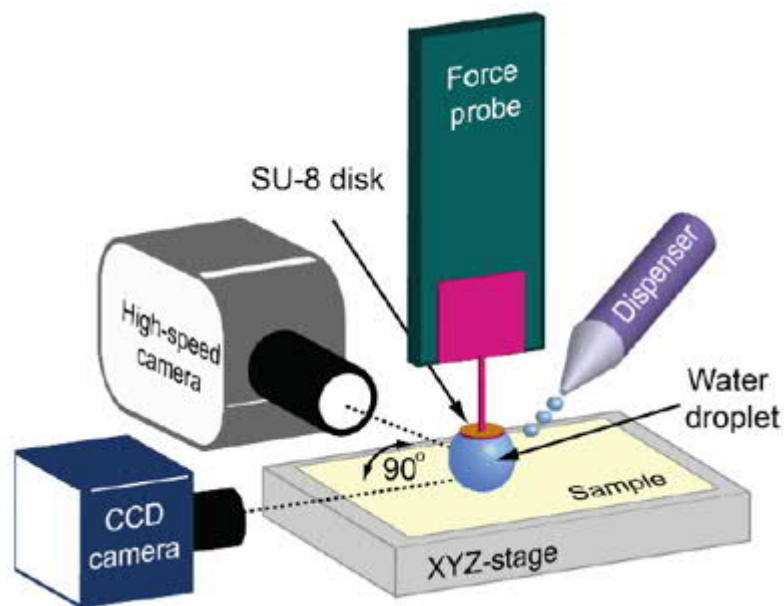

Figure 2.10 A schematic illustration of the scanning droplet adhesion microscope:
The instrument set-up is not scaled, and is showing force sensor with a SU-8 disk for holding water droplet, a dispenser used for shooting sub-μl water droplets, a high-speed camera, and a CCD camera to image the side and top views, and multi-axis automated translation stages with positing resolution down to μm [19].

Measurement procedure for a single data-point depicted in Figure 2.11. The measurement begins when the sample surface is starting to approach the water droplet, which is pinned to a force sensing probe (a-I). With constant speed, the stage in z-

direction starts moving up, towards the droplet up to the point where solid surface reaches the droplet (snap-in moment, a-II), once the droplet and sample are in contact, a step down is detected in the force (b-II). There are two approaches to keep the pushing force constant to minimize variation between measurements for all measured data-points; stage keeps moving up either for a fixed time after snap-in (called fixed time delay) or until the force reaches to a predetermined value (called preset force value). Then, the stage goes down at a constant speed (a-III) until the droplet separates from the surface (called the pull-off moment, a-IV). The pull-off force detected in the force curve (b-IV). The volume of droplets used in all experiments was 1.5 µl. For keeping the droplet's volume constant, the droplet was refilled to 1.5 µl after each measurement.
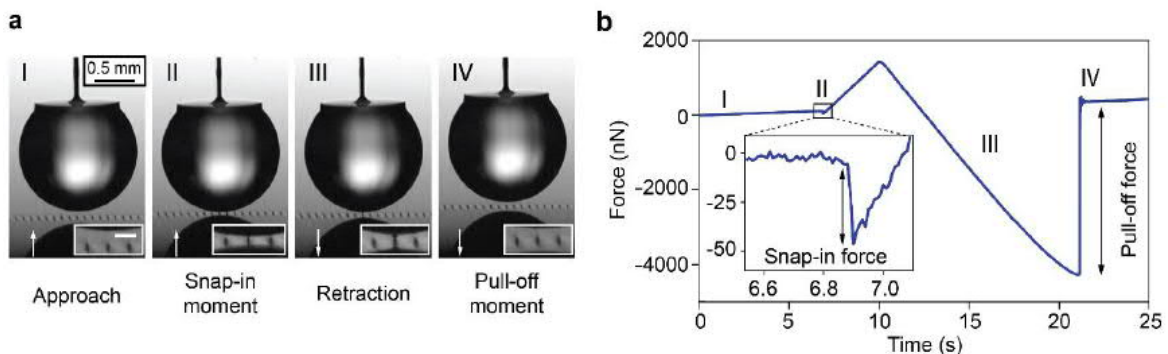

Figure 2.11 Measurement procedure for a single data point on a hydrophobic pillar:
(a) Individual measurement steps where white arrows show the direction of movement for a solid sample. (b) Force curve for a superhydrophobic surface as described previously [12].

Scanning over an area of interest is performed point by point in a defined area. Plotting snap-in and pull-off force for the scanned area will yield maps that correspond to the local wetting properties of the sample. Force maps may depend on the micro- and nanostructure of the surface, and chemical heterogeneity. Crow butterfly force maps with specific measurement intervals are shown in Figure 2.12.
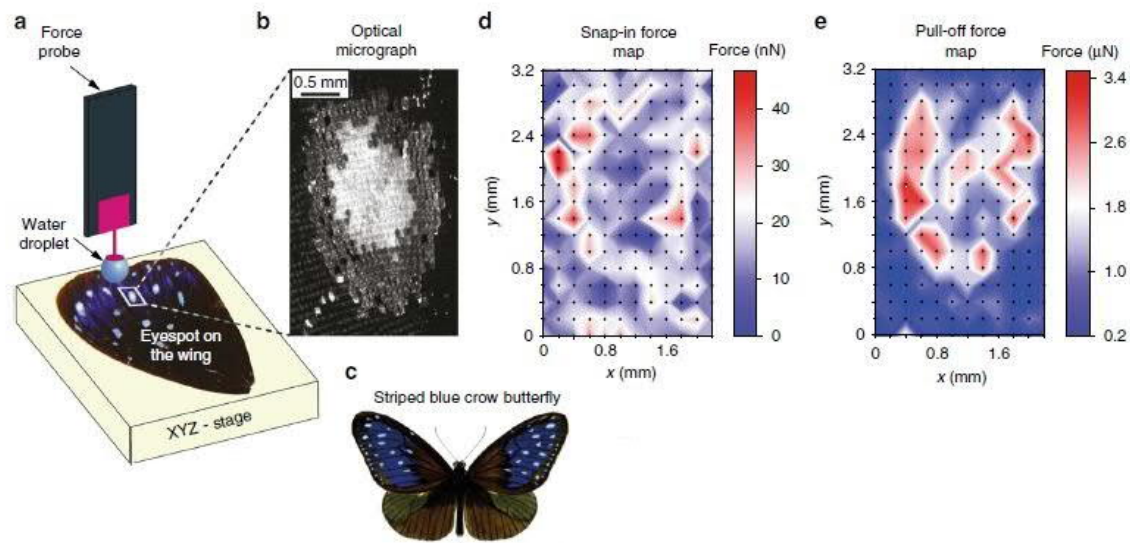
Figure 2.12 The concept of scanning droplet adhesion microscopy and provided wetting maps for a biological sample:
(a) Instrument schematic illustration. (b) Optical micrograph of scanned eyespot area. (c) Striped blue crow butterfly. (d) Snap-in force map. (e) Pull-off force map [12].

2.4.1 Scanning droplet adhesion microscopy

Scanning droplet adhesion microscopy is a state-of-the-art technique for characterizing the superhydrophobic surfaces in high precession [12]. This technique paves the way for characterizing adhesion and wetting properties of hydrophobic surfaces since high contact angle, and small variations are challenging to be measured with common optical methods [12]. While other force-based methods suffer from low sensitivity and spatial resolution, scanning droplet adhesion microscopy can provide wetting maps in nN order force resolution with high spatial resolution down to 10 μm [12]. As described in section 2.3.2, characterizing the wettability of superhydrophobic surfaces can be done by studying adhesion forces when the droplet interacts with the surface. Adhesion work is involved not only in the separation of liquid from a surface (corresponds to pull-off force) but also when a droplet brought into contact with a surface (corresponds to snap-in force). In other words, the work of adhesion in the normal direction can be considered as a reversible work when a hanging droplet brought in contact with a solid surface and then separated. As described in Equation (2.9), the work of adhesion can be estimated from contact angle and surface energy. Besides, different practices have revealed there is a relationship between dynamic contact angle, snap-in and pull-off forces [12][13].

Unique sensitivity allows quantification of wetting variations on the water repellent solid surfaces. The high spatial resolution of 10 μm paves the way for obtaining wetting

inhomogeneity maps on non-flat surfaces and biological samples. The instrument is capable of doing measurements with high accuracy and repeatability. However, this method is prone to some limitations; (1) the samples should necessarily have superhydrophobic wetting characteristics (θ_c>150°) with low adhesion forces; (2) the force sensing probe is very fragile, and if the sample surface has hydrophilic pinpoints, it might not be possible to generate wetting maps.

2.5 Conclusion

Currently, optical contact angle measurement considered as a gold standard for the characterization of surface wettability [27]. Although both static and dynamic contact angle can be measured for a wide range of surfaces by this method, repeatability and accuracy are still challenging, especially for rough, superhydrophobic surfaces. Once the contact angle reaches 180°, the uncertainty of 1μm in detecting the location of the baseline can result in 10° inaccuracy in the measured contact angle [20]. In addition, many attractive natural superhydrophobic surfaces, such as plant leaves or insect wings, have curved surface topography that direct optical methods are unable to detect the baseline [18]. Another approach to wetting characterization is the Wilhelmy plate method. While the Wilhelmy plate method can provide advancing and receding contact angle quite accurate, the absolute error of 1 μN in the measured force will lead to uncertainties up to 10° degrees for contact angles higher than 175° [33]. On the other hand, the fabrication of identical, homogeneous surfaces required for sample preparation, attached to both sides of the plate, is challenging. Furthermore, submersion of the plate into liquid makes this method unsuitable for wetting characterization on different spots of the sample.

In addition to challenges mentioned for contact angle and Wilhelmy plate methods, they are suffering from inaccuracy and low spatial resolution for superhydrophobic surfaces.

An alternative approach for characterizing the wettability of superhydrophobic surfaces is to study adhesion forces. Scanning droplet adhesion microscopy is a novel technique for measuring adhesion forces between the water droplet and superhydrophobic surfaces. Exceptional force sensitivity, three orders of magnitude better sensitivity than state-of-the-art methods, allows precise measurement of wetting variations on superhydrophobic surfaces. Spatial resolution down to 10 μm makes it possible to plot high-resolution snap-in and pull-off force maps for challenging superhydrophobic surfaces even on the non-flat or biological surfaces.

3. EARLY-STAGE SDAM MECHATRONICS DESIGN AND LIMITATIONS

The scanning droplet adhesion microscope is a state-of-the-art technology for wetting characterization. There are many aspects associated with instrument development, and many iterations have been planned to improve both performance and application. This chapter describes the initial mechatronics design for a better comprehensive understanding of the system. Besides, the most critical limitations in early-stage SDAM proof-of-concept will be discussed in this chapter.

The instrument divided into different modules, such as a micro-force sensor with a liquid droplet probe, a micro dispenser , multi-axis sample stages, side and top-view cameras. Every single module's functionality will be discussed in detail, and associated limitations will be described individually.

3.1 Overview of the SDAM mechatronics design

The scanning droplet adhesion microscopy is the result of a collaborative research effort of Robotic Instrument research group and Soft Matter and Wetting research group at Aalto University. Droplet adhesion force microscopy set-up was developed in house with commercial off-the-shelve components and custom-built control software. The set-up comprises a stationary micro-force sensor with a liquid droplet probe (e.g., water), as shown in Figure 3.1. A micro dispenser with a piezoelectric actuator used for dispensing sub-microliter droplets. The dispenser needs to be aligned with the force sensing probe in a way that the dispensed droplets bounce a superhydrophobic surface off and hit the droplet hanging-disk made out of SU-8. While the force sensing probe is a stationary module, a multi-axis positioning stage moves the solid sample in XYZ directions (3DOF).

It has been experimentally proven wetting properties can be characterized by droplet adhesion forces, e.g., resistance to detaching a droplet in the normal direction [12][13][33]–[35]. For approaching the solid samples towards the liquid droplet probe, and retraction of solid surface and droplet (adhesion) high-precision linear stage in Z-direction is essential. Measuring adhesion forces is possible point-by-point in a fully automated manner with high repeatability.

Superhydrophobic surfaces often contain microscopic irregularities in surface texture and chemical composition. Wetting maps obtained through droplet adhesion forces is a new approach to visualize local variations in wetting. To scan the sample's surface and generation of wetting maps, high-precision linear translation stages in XY directions

provide essential motion in the horizontal plane.

Measurements are monitored from the two sides, perpendicular to each other by a high-speed camera and a CCD camera with microscope lenses to monitor the force sensing probe and the contact between sample and water droplet. A top-view microscope camera is mounted for observing the sample surface. The instrument set-up is installed on a passive vibration isolation table since the microscope is sensitive to vibration and noise.
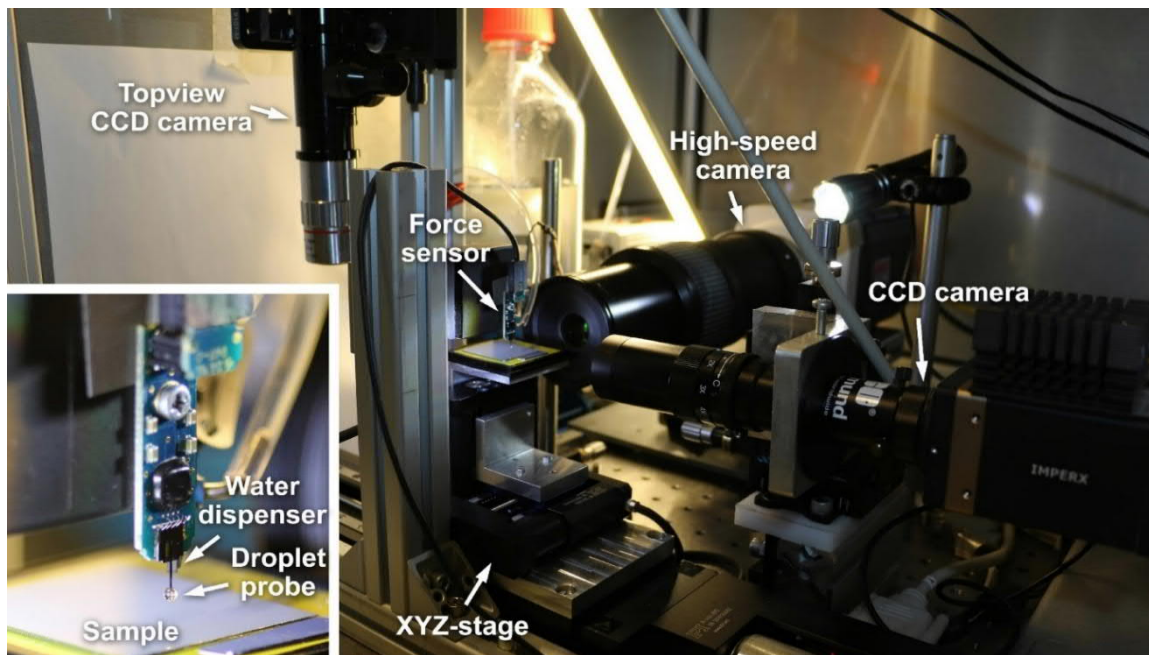

Figure 3.1 Droplet adhesion force microscope. Inset shows a close-up of the force sensor with a liquid droplet probe:
Automated high-precision linear stages in XYZ directions moves the sample towards a stationary force sensor with a liquid droplet probe. Side-view cameras for monitoring measurement procedure and a top-view microscope camera for sample surface observations are mounted [12].

3.1.1 Micro-force sensor with a liquid droplet probe

Force sensors are devices for measuring interaction forces. Strain gauge, piezoelectric, capacitive, and vision-based sensors are among the most common techniques for micro-force sensing with high resolution and stability [38]. Typically, there is a sensing element in the force sensors, which deforms when external forces are applied. Due to deformation or deflection, specific properties of the sensing element will change, e.g., resistance in strain gauges or capacitance in capacitive sensors. Change in sensing element properties will be converted into force through knowledge of sensor mechanical properties and calibration process.

Capacitive force sensors work based on variable capacitance. Applying force will vary the distance between two conductive plates, which results in capacitance change. The capacitance between two conductive plates is a function of the plates' distance d, area A, and the permittivity of the dielectric medium ε_r, and permittivity of the dielectric vacuum ε_0 based on Equation (3.1).

$$C = \varepsilon_0 \varepsilon_r \frac{A}{d} \qquad (3.1)$$

The distance between plates d is usually the variable exploited for force sensing, but the active capacitor area A can also be used.

Capacitive force sensors are more stable and sensitive in comparison with strain gauges and piezoelectric force sensors. Moreover, the capacitive force sensors exhibit no hysteresis [39]. For micro-force sensing applications, MEMS is the most common method for using the capacitive principle for force sensing [40]–[43]. A differential capacitive micro-force measurement, where two capacitors with a shared moving membrane are arranged in a parallel circuit structure is shown in Figure 3.2. A series of combs are used for maximizing A, and no dielectric material is used. When a compression force is applied on the tip, the combs on the left of the image will grow apart, decreasing in capacitance. The combs on the right will increase in capacitance as they get closer. The voltage difference due to changes in two capacitors can be calculated through Equation (3.2). A differential architecture facilitates the linearity of the measuring electronics, usually through a Wheatstone bridge [41], as well as decreasing the sensitivity to external factors [44].

$$V_0 = V_s \times \frac{C_1 - C_2}{C_1 + C_2} \qquad (3.2)$$

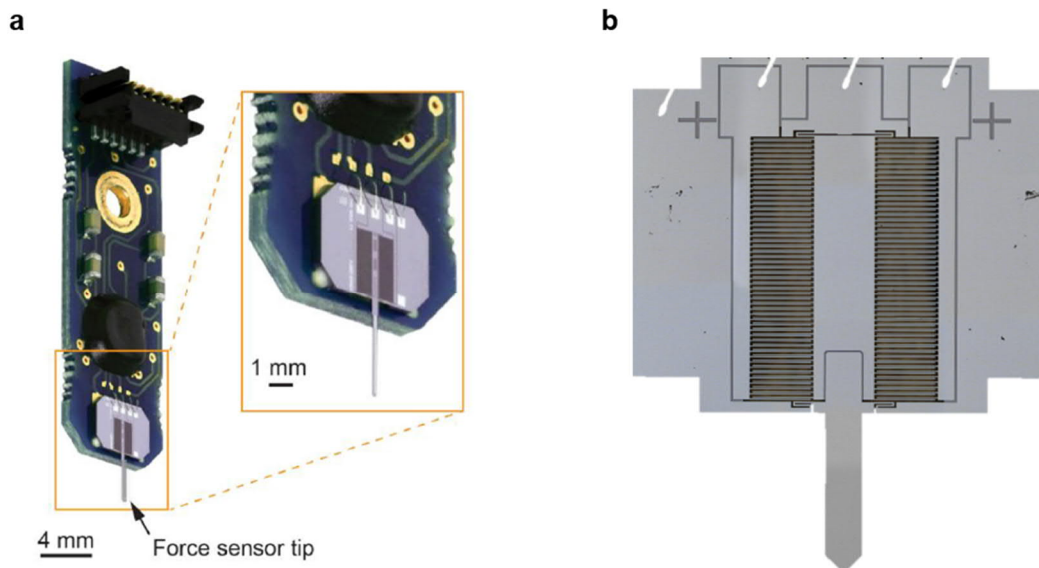Where V_0 is the output voltage, V_s is the supply voltage, and C_1 and C_2 are capacitances.

Figure 3.2 Capacitive micro-force sensor manufactured by FemtoTools AG, Switzerland: (a) Photograph of micro-force sensor FT-S100, force range ± 100 µN showing the sensor tip and MEMS combs structures. (b) Optical microscope image of MEMS structure with two series of fixed combs on the right and left side and a shared moving membrane and force sensing tip arranged in a parallel circuit [45].

Force sensing probe is the core technology of scanning droplet adhesion microscope, which consists of a micro-force sensor, liquid droplet probe, and DAQ board. The micro-force sensors (FT-S100, range ± 100 µN and FT-S1000, range ± 1000 µN; FemtoTools AG, Switzerland) with resolution in Nano-newton order, is used for developing liquid droplet probe. The micro-force sensor is capable of measuring both tension and compression forces and works based on variable displacement capacitors.

The output signal is 0-5 volts, and base voltage (output signal without any load) is 2.25 volts. Analog to digital DAQ board is used for acquiring and conversion of the continuous output signal to digital. However, one always need to compromise between resolution and sampling frequency rate. Once the sampling frequency rate increase (from 10 Hz to 1000 Hz), the resolution will drop by 10 times in theory (from 5 nN to 50 nN).

A droplet-hanging disk is made out of SU-8 and glued to the tip of the micro-force sensor to facilitate pinning a microliter droplet to the force sensing probe. Hydrophilic wetting characteristics of the hanging-droplet disk result in pinning the dispensed droplets to the disk (liquid droplet probe).

3.1.2 Microdispensing module

The dispensing is an operation during which a specific liquid is taken from a reservoir and divide into smaller portions in such a way that the size of the portions can be controlled. Chemistry, biology, and medicine are taking advantage of systems with reduced sample volume such as micropipettes and micro dispenser s. Also, dispensers used for non-contact dispensing, which keeps the doors open for many applications like inkjet printers.

In SDAM, the dispensing module is implemented for non-contact droplet formation on the force sensing probe and refill it to compensate the liquid evaporation over time. The deposition of the droplet on the modified probe is done by shooting sub-microliter droplets via the piezoelectric micro dispenser . The small droplets bounce off a superhydrophobic surface onto the disk, accumulating into larger droplet used in the measurements with a constant volume of 1.5 µl. The droplet's volume is controlled through the force given by the sensor. The dispensing process will be suspended once the weight of the hanging droplet reaches the defined force threshold in control software.

There are different dispensing technologies such as valve type dispensers, pump type, pneumatic time-pressure, and capillary dispensers. Capillary type dispensers comprise of a capillary with small piezoelectric actuators, which is the dominant technology used in micro dispensers.

The micro dispenser is used for non-contact droplet formation in the SDAM set-up. The dispenser works based on the drop-on-demand principle. When the piezoelectric actuator is triggered, a silicon diaphragm behind the actuator will bend, which leads to compression and ejection of a droplet from the nozzle. Once the actuator discharged, it will return to its initial position, and the dispenser will refill with liquid from the inlet.

The dispenser is manufactured by etching a channel in the silicon, and glass is anodically bonded. The dispenser is cut out from the wafer, as shown in Figure 3.3. Piezoelectric actuator and cable plug are attached, and the pipette mounted in the PEEK housing.
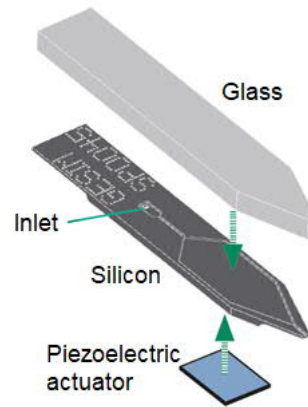
Figure 3.3 Micro dispenser manufactured by GESIM Company, GmbH, Germany:
A Channel etched in the silicon, and a piezoelectric actuator attached to the other side. Applying a voltage pulse to the piezoelectric actuator contracts and creates a pressure pulse in the liquid inside the channel and results in the ejection of a droplet from the nozzle [46].

The dispensers also called pipettes or jets, follow the drop-on-demand principle; i.e., a drop is released precisely when the piezoceramic actuator is triggered. This results in the bending of a silicon diaphragm behind the actuator and, in turn, leads to a compression of the liquid inside the pump chamber and hence to the ejection of a droplet from the nozzle. The actuator returns to its initial state, and the dispenser is refilled with liquid from the inlet. No valve is involved in this process.

The main challenges with the described micro dispenser are fragility and high cost. In capillary type dispensers, the capillary and actuator are integrated. Either contamination of capillary or damage to the actuator will force the user to change the dispenser head.

Contamination can easily result in blocking the dispenser's outlet. If the dispenser's head is clogged, usually, the users forced to increase the actuation voltage to induce higher stroke by the piezoelectric actuator. This action might work in conditions that the path is not entirely clogged, and it might solve the problem for a short time, but high-voltage actuation ultimately will result in breaking the actuator and consequently dispenser head. Meanwhile, cleaning the dispenser's head in ultrasonic cleaners is challenging due to fragility and the small size of the dispenser head.

3.1.3 Positioning module

Although the micro-force sensor is the core technology of SDAM, automated positioning modules are also critical. The force sensing probe is a stationary module to minimize the noise level. Any force sensing probe's movement will result in liquid droplet probe vibration and signal oscillation. Therefore, the positioning module is intended to move

the sample in XYZ directions with high-repeatability and accuracy. The measurement procedure is associated with approaching the sample towards the force sensing probe and retraction at the constant speed, 5 $\mu m.s^{-1}$ in Z-direction (explained in Chapter 2; Section 2.4). The movement in XY directions is necessary for scanning the surface to generate force maps.

Three motorized high-precision translation stages For X-direction (M-404.8PD, 0.50 μm precision, Physik Instrumente GmbH, Germany), Y-direction (M-122.2DD, 0.15 μm precision, Physik Instrumente GmbH, Germany), and Z-direction (M-111.1DG, 0.10 μm precision, Physik Instrumente GmbH, Germany) are arranged as shown in Figure 3.1.

The most critical translation stage in this configuration is the one in Z-direction since the final vertical position defines the pushing force in a fixed time delay control approach, discussed in Chapter 2; Section 2.4. Also, the positioning accuracy and repeatability in Z-direction can guarantee the force curves for different points are collected at the same measurement condition. Any inaccuracy in XY directions will result in a force map's error.

3.2 Critical limitations in early-stage SDAM proof-of-concept

Although the ability of early-stage SDAM is very attractive in measuring microfeatures and surface inhomogeneity, the system performance has much to desire. The early-stage proof-of-concept suffers from issues such as sensor fragility and time-consuming preparation procedure. Also, the ad hoc construction of the set-up is hard to improve, and systematic design and implementation are necessary.

In summary, the following limitations need to be addressed:
1. The micro-force sensing probe is so fragile and suffers from signal fluctuation and high-rate of breakage in a short period. Overloading of the sensor will break microfabricated capacitors on MEMS, which leads to a shift in base voltage or inducing non-linearity in sensor output signals.
2. The current dispensing module is prone to contamination. Besides, fragility and uneven quality of the dispenser head lead to a time-consuming preparation procedure.
3. Inefficient alignment mechanism between dispenser and force sensing probe results in the long preparation procedure.
4. Lack of system frame design and ad hoc system configuration leave tiny free

space for positioning stages. Although the standard tray size for accommodating samples is 4×4 centimeters, the travel range in Y-direction is limited to 2.5 centimeters. In practice, almost 50% of the samples' area is not reachable.

5. The non-adaptive sample holder is a considerable drawback for SDAM as a lab instrument. The instrument needs to be adaptive to samples with different formats.

6. The current vision module does not comply with vision system design principles, which results in low image quality and high-cost. Aspects like the interplay between the camera and optical lenses, appropriate lighting, and customized alignment mechanisms are missing.

4. HIGH-PERFORMANCE MECHATRONICS DESIGN

Creating a robust and efficient instrument capable of providing accurate and repeatable measurement results is the primary objective of high-performance design. Every single module has a contribution in instrument performance, and specific attention needs to be taken into design steps and their sequence.

The mechatronics design is a sequential process in which a design solution is generated by following a series of prescribed steps start from system requirements and continues to validation [47][48]. The V-model is one of the standardized design models for mechatronics, which composed of two main phases: the top-down and the bottom-up phases. In top-down steps, the main focus is on system requirements, specifications, and conceptual design based on requirements. The detailed design is a bridge between top-down and bottom-up phases. The main effort for validation will be placed in the bottom-up phase, which aims to integrate designed modules gradually and validate the design during the entire process as depicted in Figure 4.1.
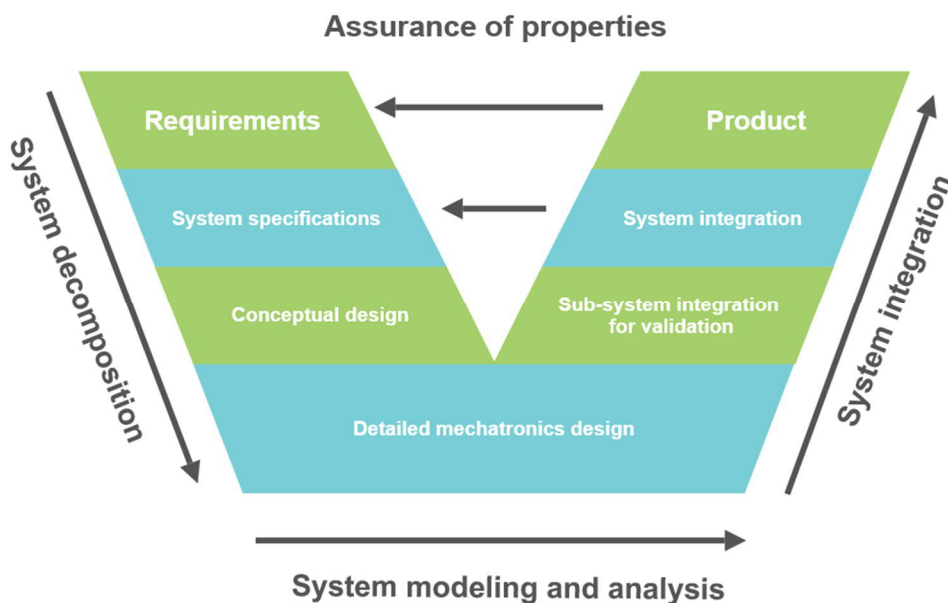

Figure 4.1 The V-model for mechatronics system design and development

A comprehensive understanding of requirements is essential to provide the desired system. The requirements should be categorized in different levels, such as system and subsystem requirements. While the system requirements define the overall system architecture, the subsystem requirements mainly concern detailed mechatronics and

modules' design. The system requirements for new SDAM are structured as follows:

1. improvement in instrument preparation time from a couple of hours to minutes through selected mechatronics modules, and efficient system configuration
2. Implement the modular design for continuous instrument development
3. Design an adaptive system for pursuing present and future research goals

To break down the system complexity, the system divided into several subsystems such as sensing module, dispensing module, positioning, and vision modules. Then, the detailed design process for modules is discussed in the following sections. The author does all the detailed design during the TUTLI SDAM project at Aalto University, and the work is extended to the system performance evaluation (chapter 5).

The main contributions of the author presented in this chapter are as follows.

1. Instrument architecture, conceptual design, and detailed mechatronics design
2. System 3D modeling, technical drawing for part manufacturing, and set-up assembly for a new SDAM
3. Selection of high-performance micro dispenser, module integration, and performing experiments such as droplet volume accuracy, surface tension, and chemical resistivity
4. Vision system selection, microscope camera, and module integration
5. Alignment mechanism design for microdispensing and vision modules
6. Selection of automated translation stages for multi-axis sample positioning, and module configuration (3 DOF)

4.1 Dispensing module design

The dispensing refers to an operation in which the liquid is released in a specific portion in a controllable manner. In the present work, the micro dispenser relates to the system that is capable of distributing liquid volumes in the magnitude of microliters or less (<1µl).

In SDAM, the dispensing module is needed for forming the droplet attached to the force sensing probe and refilling the droplet to compensate the liquid evaporation over time. The integration of a robust dispensing system into the SDAM instrument can improve the system performance significantly. The requirement for the dispensing module is as follows:

*   Dispensing droplets in micro –and nanoliter order for droplet formation (1.5 µl) and droplet refilling

- High-chemical resistivity of fluidic path
- High droplet volume accuracy
- High dispensing frequency to minimize the working time

A robust dispensing technology that complies with SDAM requirements is selected. Oppose to the majority of micro dispenser s, in which the capillary and piezoelectric actuator are integrated (described in chapter 3; section 3.1), in the chosen dispenser, the fluidic path and actuator are entirely separated. This feature plays an essential role in both the performance and robustness of the dispensing module. The capillary is a disposable part, which installs in a clamp, and the actuator squeezes the nozzle with a defined stroke at a specified frequency, as shown in Figure 4.2.
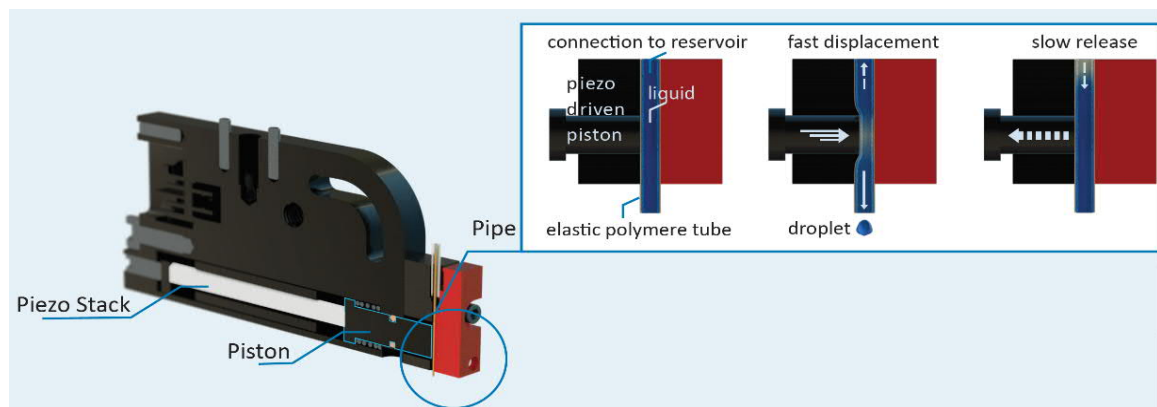

Figure 4.2 Schematic illustration of micro dispenser manufactured by BioFludiX Company, GmbH, Germany:
There is a piezoelectric actuator, which induces a stroke to the flexible nozzle through a dynamic piston [49].

Disposable and flexible nozzles have advantages over conventional capillary glasses. The blockage of the fluidic path over time is one of the main concerns with conventional micro dispenser s. Due to fluidic path blockage, the dispenser performance will drastically drop. As described in the previous chapter, inducing higher stroke by an exciting actuator with higher voltage will result in breaking the actuator and consequently dispenser head.

Besides, disposable nozzles, shown in Figure 4.3, provides the user with a wide range of compatible nozzles with a universal actuator. Different nozzles in diameter (125 … 500 μm) are designed for dispensing in various volumes (1 … 70 nl). Oppose to miniaturized actuators used in conventional micro dispenser s, the need for micropumps is eliminated by implementing powerful actuators.
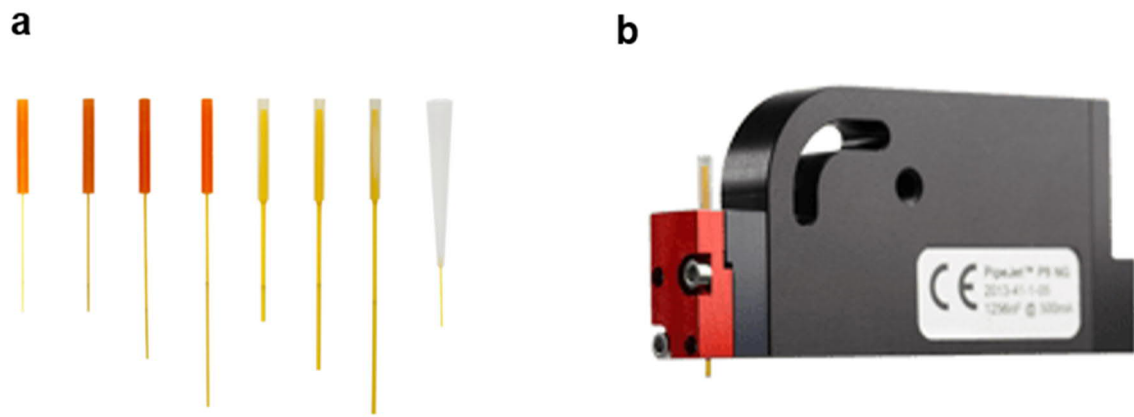
Figure 4.3 Variety of disposable nozzles that are compatible with a single actuator:
(a) Available nozzles have a different internal diameter designed for dispensing a specific range of droplets (1 … 70nl). (b) A single piezoelectric with a universal clamp to mount different nozzle [49].

The dispensing event is subdivided into three phases, as shown in Figure 4.4. In the first phase called charge time, the piezoelectric actuator expands to the specified stroke. Due to applied stroke to the flexible nozzle, the liquid is displaced in the tube, and a jet of droplets will form at the nozzle outlet. In the second phase known as hold time, the actuator movement will suspend, and the droplet will tears off. In the last phase called discharge time, the actuator retracts, and a portion of liquid refilled into the relaxed nozzle by capillary forces. Corresponds to the number of shots dispensing cycle will be repeated, and the dispensing frequency will define how fast the entire dispensing cycles will be. There is a short delay (100 ms) between each dispensing cycle.

Piezoelectric deflection distance correlates with the dispensed volume, and it can be reached by charging of the actuator. The downstroke velocity (i.e., the velocity at which the piston squeezes the nozzle correlates with kinetic energy. For instance, increasing downstroke velocity will result in dispensed droplets with higher kinetic energy. Besides, if the velocity is too low, no droplet will tear off, and if it is too high, satellite droplets may appear. Typical values range from 60-100 $\mu m.ms^{-1}$ for water-based samples is recommended.
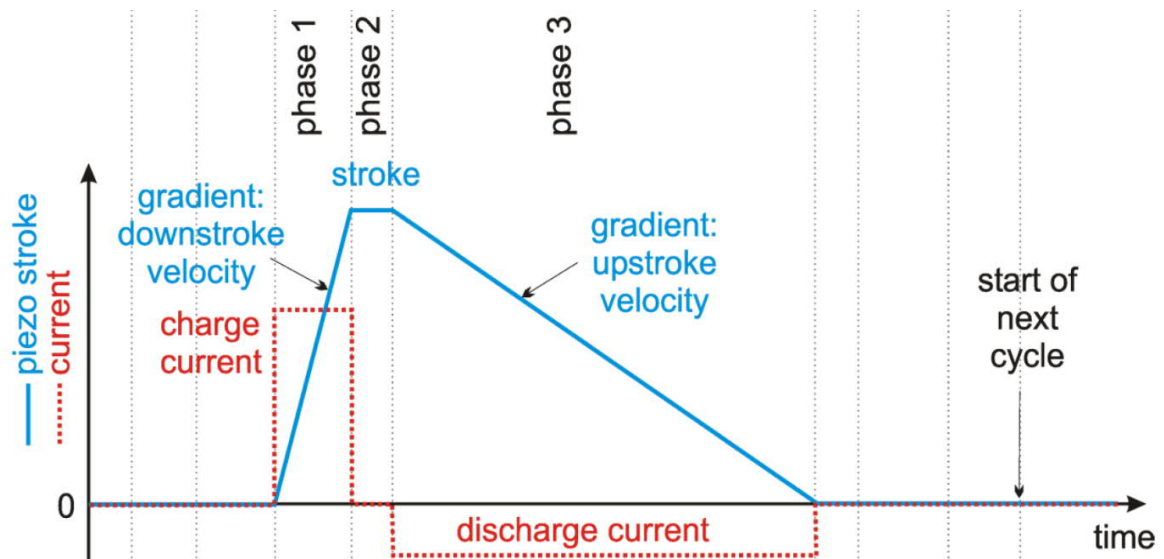
Figure 4.4 Single dispensing cycle divided into three phases [49]:
In phase 1, the current charge will result in piezoelectric actuator expansion, and the downstroke gradient mainly defines the dispensing quality. In phase 2, the stroke will halt for a specific time, and the droplet will tear off. In phase 3, the retraction of the actuator results in nozzle relaxation and liquid refill.

4.1.1 Fluidic path chemical resistance

The integration of this technology into SDAM needs some considerations such as fluidic path chemical resistance, droplet volume accuracy, and alignment mechanism design. Adhesion force is a function of liquid surface tension, described by Dupré's Equation (2.8). Fluid contamination will result in considerable changes in surface tension and adhesion force, consequently. To make sure the nozzles, tube, and reservoir (components in contact with liquid) made out of high-quality materials, which are chemically resistant, the liquid surface tension was measured by the pendant droplet method.

4.1.2 Droplet volume accuracy

Droplet volume accuracy is one of the crucial aspects of our application. Error in dispensed droplets' volume leads to volume deviation of the formed droplet, attached to the force sensing probe. Droplet size correlates with spatial resolution and adhesion force. Error in droplet volume causes inconsistency in measurement conditions. For keeping droplet volume consistent, the droplet refills to 1.5 µl after each measurement (described in section 2.4). By refilling, the aim is to compensate the liquid evaporation and keep the contact area constant (between droplet and sample).

40

The comprehensive tests were done to measure the droplet volume accuracy of the dispenser. The force sensing probe is capable of measuring the force down to 5 nN resolution. By forming the droplet attached to the force sensing probe, the droplet weight can be obtained with high accuracy.

Conversion of droplet weight W or reading force values into volume V can be done simply by Equation (4.1) where ρ is water density for Milli-Q water, assumed as 0,99 g.cm^{-3}, and g is the acceleration due to gravity, considered as 9,8 m.s^{-2}.

$$V = \frac{W}{\rho g}$$ (4.1)

The nominal dispensed droplet volume and quantities can be defined through the dispenser's GUI. Dispensed droplets will accumulate on the force sensing tip, and the ultimate force value for different droplet volumes can be found in Figure 4.5. The nominal force value for all tests is 10.5 μN. For convenience, the number of dispensed droplets and their theoretical volume for each test is presented next to it. In an ideal condition, obtained force values would be at the same level as nominal forces, which presented with the blue line at 10.5 μN in Figure 4.5.
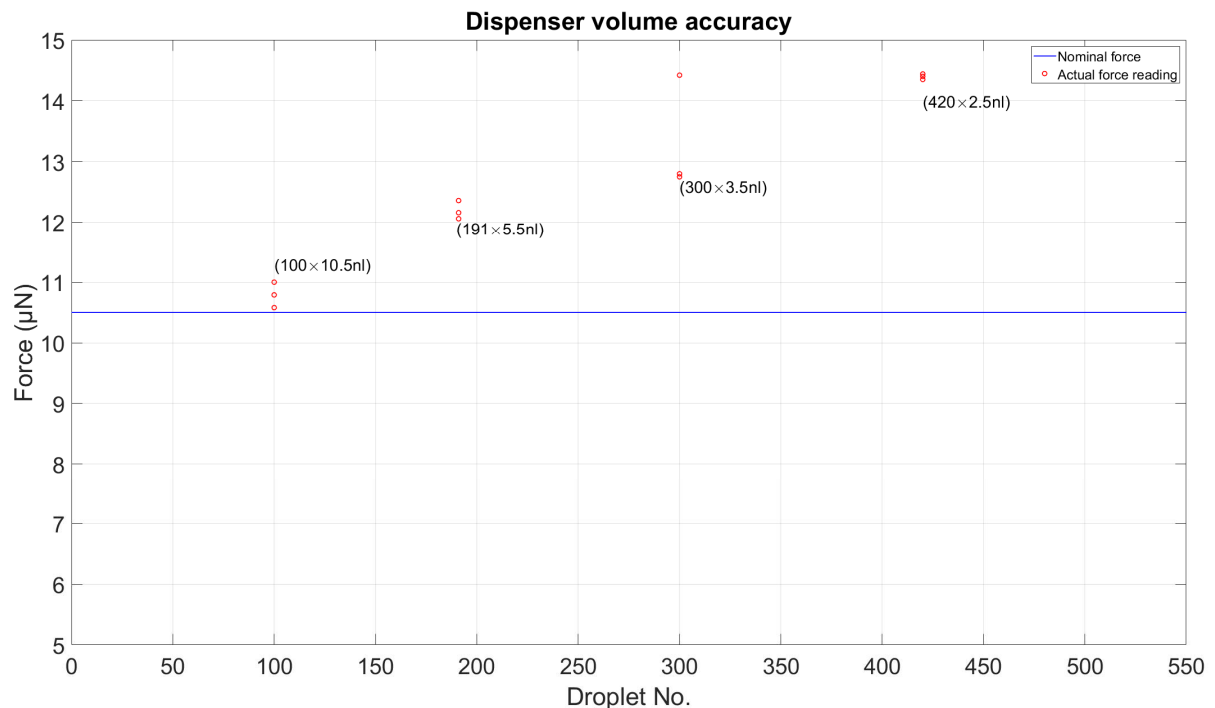

Figure 4.5 Dispenser volume accuracy for different dispensed volumes:
The nominal dispensed volume (multiplication of droplet quantities by individual volume) for all four cases are the same. Volume inaccuracy increases by minimizing individual droplet size, and higher droplet volume has the least deviation from nominal force value.

Due to dispenser volume inaccuracy, the experimental force values obtained from the micro force senor show significant error in droplet volume accuracy. Inaccuracy in volume will increases with smaller individual droplets.

4.1.3 Dispenser alignment mechanism

Kinetic energy plays a vital role in non-contact droplet formation. The sub-microliter droplets shoot to an extremely fragile force sensing probe to form a droplet with 1.5 µl volume. If the kinetic energy of dispensed droplets will be high, the micro force sensor MEMS might break. On the other hand, low energy droplets make the dispensing process challenging.

Droplets bounced off a superhydrophobic surface need to have minimum required energy to continue their motion towards force sensing tip. Otherwise, they will not hit the force sensing probe. The optimized droplet size with sufficient kinetic energy found experimentally. The distance between nozzle and force sensing tip, shooting angle, and actuation parameters (e.g., downstroke velocity and current charge magnitude) will result in different droplets' volume and kinetic energy. Several experiments were done to find the optimized distance between dispenser and force sensing probe (12 mm ± 1), shooting angle, and dispenser parameters.

Due to the deviation in nozzles geometry, the trajectory of the droplet will not always be the same. To make sure dispensed droplets will hit the droplet-hanging disk (a disk with 1 millimeter in diameter), accurate and repeatable alignment of the dispenser and the force sensing is necessary. Since the sensor is a stationary mounted module, the alignment mechanism is needed to change the dispenser position in XYZ directions (3 DOF). While changing the dispenser's position in X-direction will result in the alignment of the dispenser and the force sensing probe, movement in Y direction will lead to a change in dispenser's distance from the sensor probe. Motion in Z-direction obtained by changing vertical sample position to plan an appropriate trajectory, as shown in Figure 4.6.

 Positioning precession, repeatability, and easy access are key aspects of an alignment mechanism. Linear translation stages are designed to precisely position the dispenser along the X and Y axis with a travel range of 13 mm in each direction while the vertical positioning can be done by a change in sample vertical position with a travel range of 25 mm.
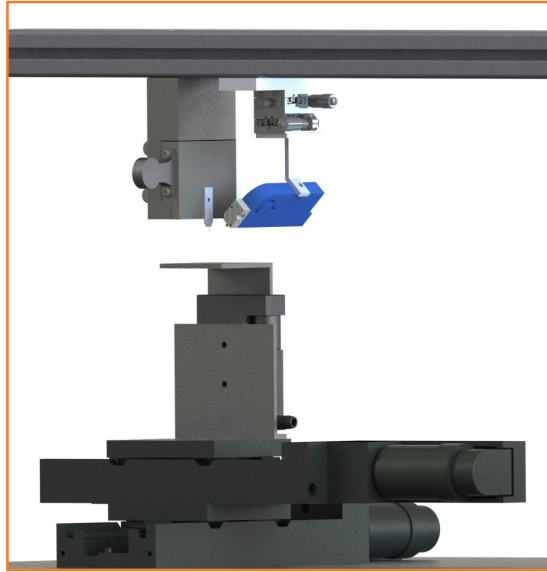
Figure 4.6 Alignment mechanism for the dispenser:
Alignment mechanism in XY direction (2 DOF) facilitates dispenser and force sensing alignment.

4.2 Vision Module

Vision module in scanning droplet adhesion microscope comprised of several microscope lenses and CCD cameras. One or two cameras mounted next to the sample holder, which captures side-view images. The primary function of the side-view camera is monitoring the force sensing probe and the droplet formation process. Imaging the contact between the sensing probe and sample surface during the measurement is another application of side-view cameras.

Besides, the top-view camera placed perpendicular to the sample surface for capturing top-view images of the sample surface. Top-view images can be useful when specific features need to be observed on the sample surface. In practice, cameras mainly used for monitoring and visual assistance of users during and after the measurement.

From a designer's point of view, two essential aspects need to be considered. First, understanding the interplay between camera sensors and imaging lenses, which is a crucial part of a vision system design. Second, an accurate and repeatable mechanism to align the microscope with a sensing probe.

4.2.1 Vision System design

Proper-paired camera and lens combination can lead to maximum image quality. Different approaches such as limiting the minimum resolvable feature size or image resolution can be followed to design a vision system based on the application. If the minimum feature size is the most crucial factor, the lens should be capable of resolving that feature. The design process begins by choosing a camera to specify the sensor resolution and primary magnification as known parameters for calculating object space resolution. In the next step, a suitable lens can be paired with the chosen camera. Alternatively, the design process can begin by choosing a lens and then pairing a decent camera. In the SDAM case, an available zooming lens in the lab is chosen, and its specifications described in Table (4.1). Zoom lenses are specified as having particular zoom ratios, which can be found by dividing the longest focal length by the smallest one for any given lens. It can also be expressed as a ratio (e.g., 6:1 or 6X).

Table 4.1 Zoom lens specifications VZM 600i manufactured by Edmund Optics Inc., USA [50].

Product	VZM 600i	Type	Zoom lens
Field of View, 1/2" Sensor	6.4 - 1.0mm	Primary Magnification (PMAG)	6:1
Field of View, 2/3" Sensor	8.8 - 1.4mm	Zoom Ratio	6:1
Maximum Sensor Format	2/3"	Working Distance	60 mm
Resolution, Object Space	87 - 176 lp/mm	Maximum Diameter	30 mm
Resolution, Image Space	87 - 29 lp/mm	Mount	C-Mount

Object and image space resolution are the key specifications to compare lenses. Object space resolution specifies the minimum feature size that the lens can resolve. For imaging resolved feature, the camera sensor should have a sufficient number of pixels with appropriate size. Object space resolution and sensor resolutions can be calculated by Equation (4.2) [51].

$$Object\ space\ resolution = Sensor\ space\ resolution \times PMAG \tag{4.2}$$

Primary magnification (PMAG) is the ratio of sensor size to the physical field of view, and it should not be confused with the zoom ratio. With different sensor size, the field of view will be different. The field of view is mentioned for two different sensor sizes in Table 4.1. Since the intention is using the maximum sensor format that the lens is

supporting (2/3"), corresponding values should be taken into account for calculating primary magnification. Equation (4.3) describes the relationship between primary magnification, sensor size, and field of view [51].

$$PMAG = \frac{Sensor\ Size\ (mm)}{Field\ of\ View\ (mm)} \tag{4.3}$$

Typically, the object and image space resolutions are defined by the frequency measured in line pairs per millimeter (lp/mm). The conversion to micrometer is possible through Equation (4.4) [52].

$$Pixel\ size(\mu m) = \frac{1000\ \left(\frac{\mu m}{mm}\right)}{2\ \times Image\ space\ resolution\ \left(\frac{lp}{mm}\right)} \tag{4.4}$$

By inserting primary magnification and image space resolution in Equation (4.2), the object space resolution for the zooming lens can be calculated.

The highest frequency that can be resolved by a sensor, the Nyquist frequency, is effectively two pixels or one line pair. By Equation (4.5), the object space resolution can be represented in micrometer [52].

$$Minimum\ resolvable\ feature\ size\ (\mu m) = \frac{1000\ \left(\frac{\mu m}{mm}\right)}{2 \times Object\ space\ resolution\left(\frac{lp}{mm}\right)} \tag{4.5}$$

Meanwhile, it worth mentioning the object and sensor space resolution values calculated by Equation (4.2) are not specify the image contrast level. Therefore, the most comprehensive method for lens performance evaluation is reviewing the Modulation Transfer Function (MTF) curves. MTF curves show resolution and contrast information simultaneously, allowing a lens to be evaluated based on the requirements for a specific application and can be used to compare the performance of multiple lenses or cameras. An example of an MTF curve for a fixed focus lens with a maximum sensor format of 2/3" showed in Figure 4.7. The curve shows lens contrast over a frequency range from 0 lp/mm to 100 lp/mm (the sensor's limiting resolution is 62lp/mm).

The MTF curves for the used lens in SDAM setup (VZM 600) are not available, and that is the reason the design is done based on Equations (4.2 – 4.5) discussed in this section.
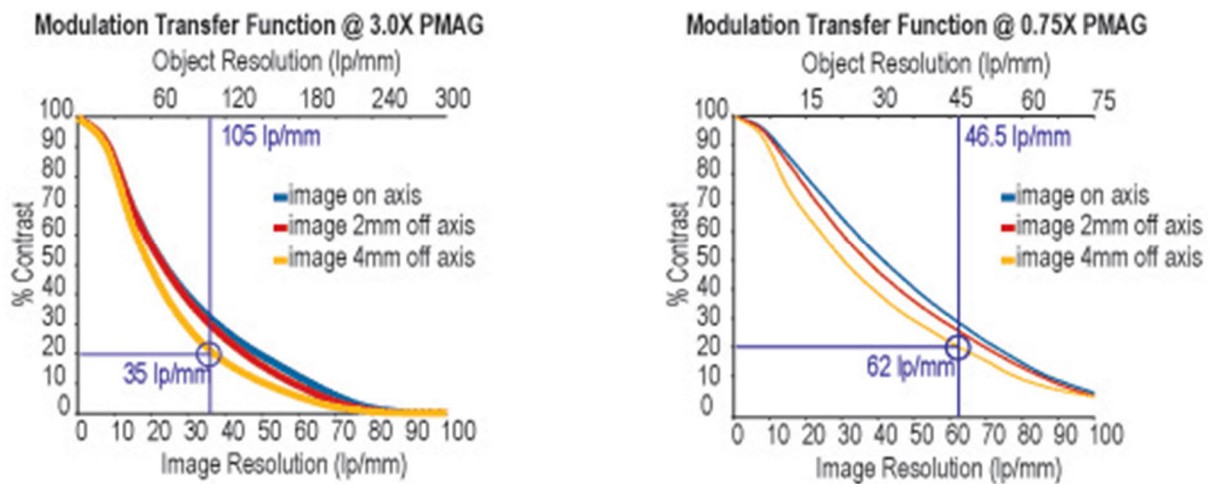
Figure 4.7 MTF Curve for VZM 300 manufactured by Edmund Optics Inc., USA [50].

4.2.2 Alignment mechanism design for the vision system

Since microscope cameras have a high-magnification and minimized field of view (8.8-1.4 mm), alignment mechanism with some degrees of freedom is essential. Positioning precession, repeatability, and easy access are vital aspects of an alignment mechanism for the vision module.

Depends on the zooming lens type (fixed focal or focus lens), free space for installing vision module, and intended view for image capturing, one could come up with a different design. A common design for microscope camera alignment, which mostly can be found in contact angle goniometer instruments has shown in Figure 4.8. The microscope camera is installed perpendicular to the dispenser tip and sample surface to capture the side view. The sample surface and camera need to be set at the same height. Thus, the adjustment in Z-direction can be made by changing either the sample or camera height depends on the implemented design for fine part adjustment in Z-direction. Besides, the distance between the camera and nozzle tip can be set by moving the entire camera mount along T-slots.

The user cannot align the camera in a lateral direction, which is a weakness for implemented camera mount design, as shown in Figure 4.8. Besides, the motion along the T-slot path is quite sharp, which forces the designers to use only variable focus zooming lenses.
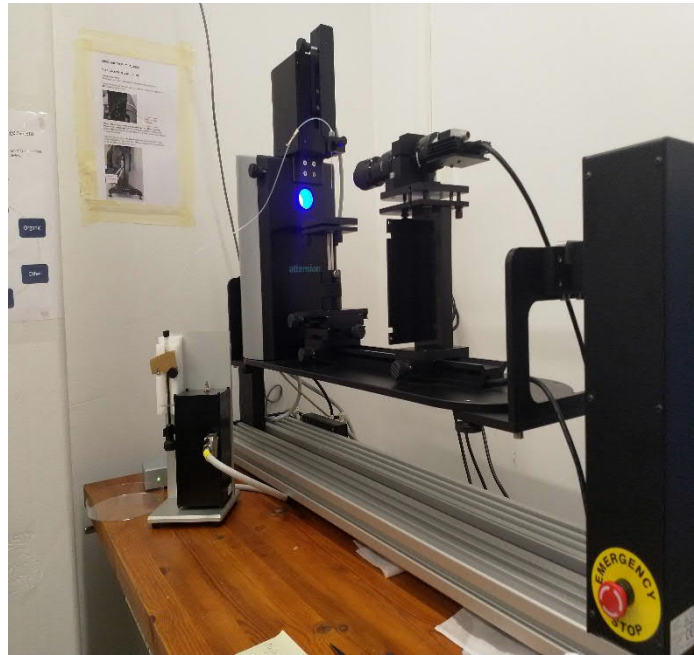
46

Figure 4.8. Contact angle goniometer manufactured by Biolin Scientific, a Nordic instruments company:
Camera position can change in T-slot direction, and lateral direction alignment can only be done by changing the sample holder position.

Considering the mentioned drawbacks, and specific needs in the SDAM instrument, an alignment mechanism is designed by combining linear translation stages to precisely position the camera along the XYZ axis. The incremental motion along X-direction provides an incremental motion of the microscope camera with a fixed focus lens for focusing on the sensor's tip. Motion in Y and Z-directions allows aligning the camera in lateral and vertical directions, respectively.

The cubic design of alignment mechanism XYZ directions (3DOF) for microscope camera implemented in SDAM showed in Figure 4.9.
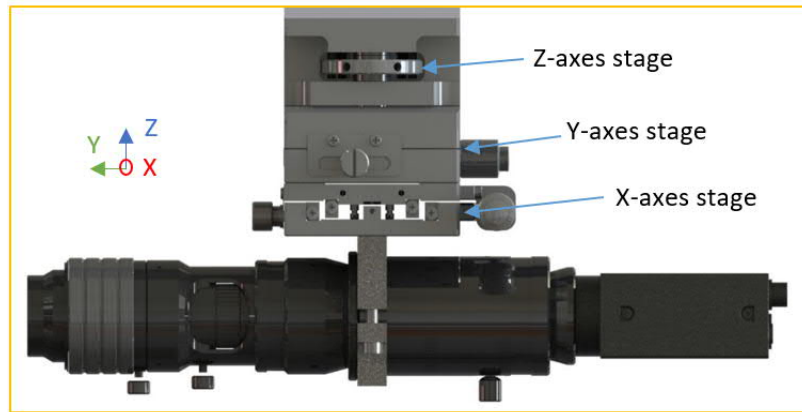
Figure 4.9 Compact multi-axis (3 DOF) alignment mechanisms design with mount, camera, and a zoom lens.

4.3 Adaptive frame design

To comply with modularity in design, the instrument is subdivided into different modules. The design process for each module is done, as discussed in previous sections of this chapter. An adaptive frame is implemented to arrange designed modules in the best configuration. During the instrument development process, upgrading the components or even the instrument reconfiguration is inevitable. Thus, the system frame should support different configurations. Also, the instrument frame should be adaptive for future modules' developments.

Installation of components like sensing, dispensing, and vision modules on the same horizontal bar are advantageous from different points of view. First, by mounting the stationary modules from the top, the movement plane of sample positioning stages is entirely free, and the danger of collision between the sample holder and other modules eliminated. In other words, the instrument bottom plane kept free of any stationary components, which makes the positioning stages' movements in maximum travel range safe, as shown in Figure 4.10.

Second, mounting stationary modules at the same level made the device compact and user-friendly. The relative distance of modules, e.g., dispenser and micro-force sensor, can be changed with ease. It also resulted in a more convenient and user-friendly alignment procedure.
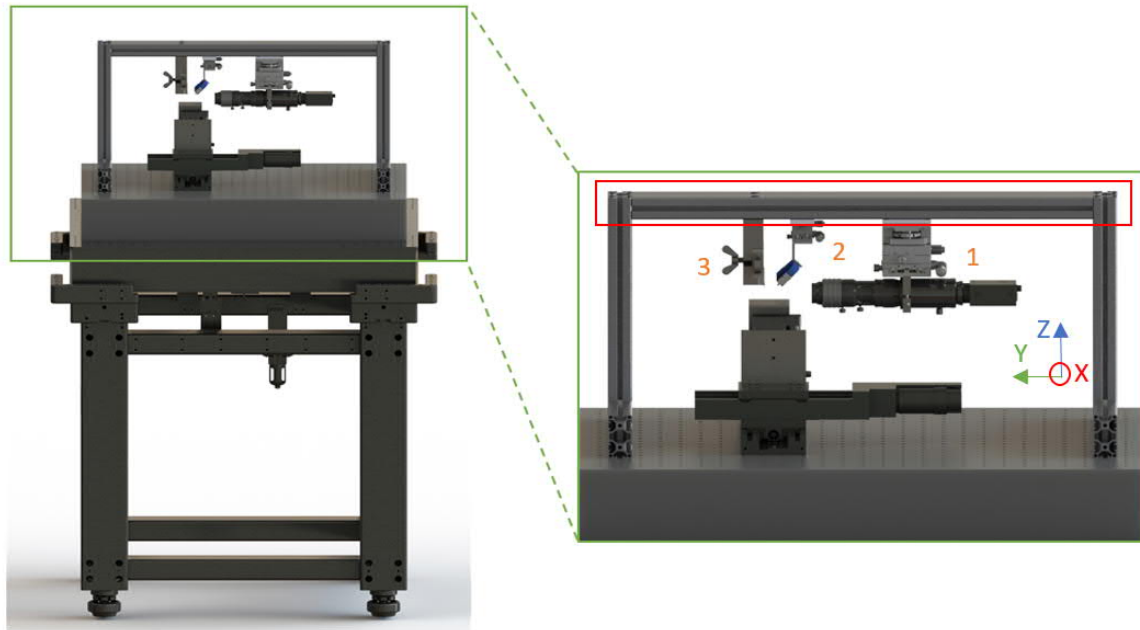
Figure 4.10 High-performance design for scanning droplet adhesion force microscope with the implementation of an adaptive frame and new system configuration:
The horizontal bar (highlighted with a red rectangle) can be adjusted in Z-direction, and stationery modules (labeled 1 to 3) can mount at any point along Y-direction, and their relative distance from one another can be changed.

Third, the thickness of the sample might vary from some millimeters to centimeters. Therefore, in the current set-up configuration, the top horizontal bar can be mounted at different levels with ease. In the new design, the position of modules can change in the XYZ axis to maximize the system flexibility and usability.

The frame is constructed by aluminum bars. The primary motivations for using aluminum bars are eliminating the manufacturing process, minimizing the cost, and benefit from high flexibility.

5.   SDAM PERFORMANCE EVALUATION

This chapter evaluates the instrument performance when the hardware and software are integrated, and the instrument can be tested in the operational mode. This chapter will then discuss the critical aspects associated with high-performance design, such as preparation procedure, instrument design, and scanning speed.

1. Instrument performance benchmarking
2. Benchmarking vibration isolation units (passive and active) against instrument vibration in operational mode
3. Performing the scanning droplet adhesion microscopy for superhydrophobic surfaces

5.1 Instrument preparation time

The instrument preparation time is considered as a measurement overhead, which needs to be minimized. To shorten the preparation time, optimizing involved modules are essential.

In early-stage SDAM, the instrument preparation time is about 1-4 hours. The main issues which result in such a significant overhead time are mainly fragile and ineffective dispensing module, and ad hoc system configuration, as discussed in chapter 3.

By systematic instrument design for new SDAM, the preparation time decreased to 15-30 minutes. Reliable dispensing technology with a high level of flexibility is integrated into setup. Also, alignment mechanisms are designed to speed up the preparation process, as shown in Figure 5.1.

Due to sensor fragility, a portable sensor holder is designed and manufactured, which makes the force sensor installation safe, and fast. Handling and mounting the micro-force sensor was previously challenging, and the user obliged to handle and install it with a lot of considerations.
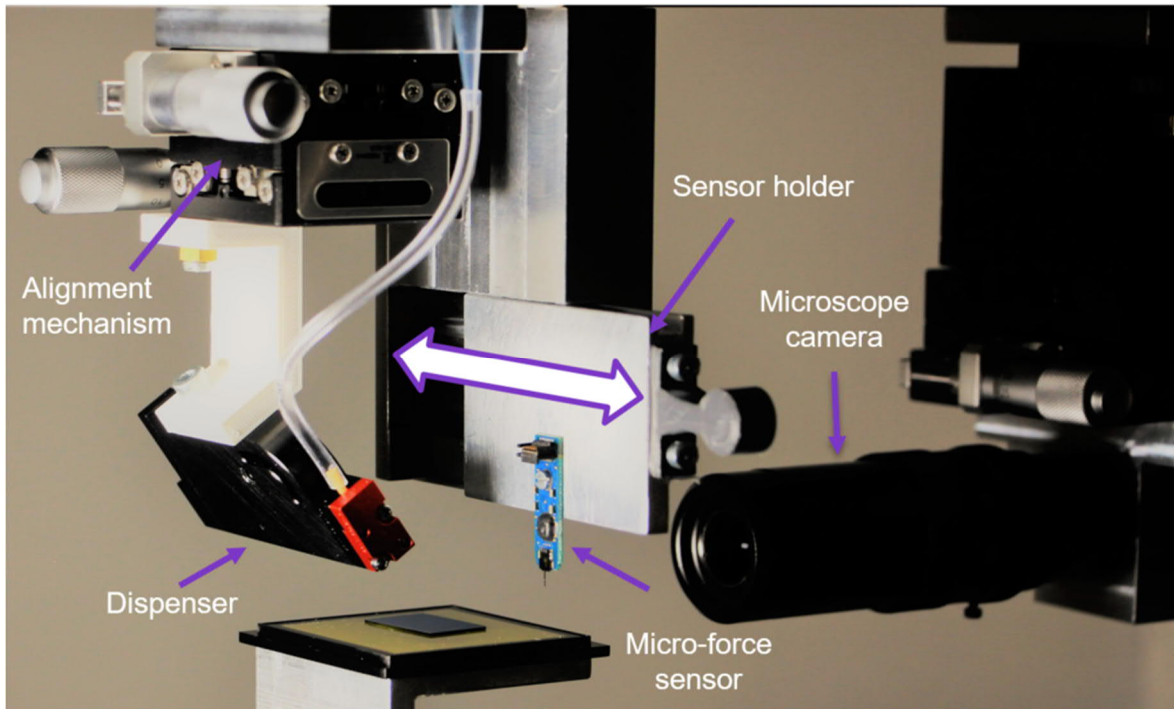
Figure 5.1 New instrument close-ups view:
Micro-force sensor attached to the portable sensor holder for secure installation where dispenser configuration and alignment mechanism has shown

5.2 Instrument scanning speed

High scanning speed is desirable for SDAM, especially for high-resolution wetting maps. For instance, the generation of the wetting map with a 50×50 data points takes almost 40 hours in early-stage SDAM. To maximize speed, one needs to optimize the measurement procedure. Table 5.1 describes the measurement steps and corresponding time for an individual point measurement.

Table 5.1 Procedure for measuring individual points and corresponding time (Approach and retraction at 5 μm.s-1)

Measurement step	Allocated time (Unit)	Allocated time (unit)
Force initialization	6 (second)	10 %
Approach and retraction	30 (second)	50 %
Droplet refill	12 (second)	20 %
Neutralization	12 (second)	20 %
Total measurement time for an individual point	60 (second)	100 %

The approach and retraction of the sample take 50% of the measuring time. Therefore, any improvement can significantly boost the scanning speed. The effect of approach speed on the snap-in force and the impact of retraction speed on the pull-off force have been studied by scientists to define the optimum approach and retraction speeds. The obtained results reveal snap-in force grows when the approach speed is increasing while the pull-off force is much less sensitive to retraction speed [12]. The results for approach and retraction speed characterization can be found in Appendix 1.

Fine motion stages that can simultaneously produce high-speed motion (50 mm.s^{-1}) are implemented for SDAM to improve the scanning speed. However, the optimum approach and retraction speed (5 µm.s^{-1}) is the main limiting factor. More experiments on different superhydrophobic surfaces are essential to finding a comprehensive understanding of the wetting mechanism for further developments.

An amplitude spectrum measurement is done to determine the vibrational levels for SDAM by utilizing a six-channel spectrum analyzer. Three piezoelectric ICP accelerometers, broadband resolution of 1 µg, are mounted in XYZ-directions for noise measurements.

Figure 5.2. Six-channel spectrum analyzer and XYZ-directions piezoelectric ICP accelerometers.

A set of measurements is carried out to consider the effect of ground vibration and induced vibration due to stage motion. The stage motion during approach and retraction will cause vibration, which can increase the noise level in force curves. Therefore, the vibration level against different approach and retraction speeds are measured while the instrument installed on top of the passive vibration isolation tables, and active isolation benchtop, as results shown in Figures 5.3 and 5.4.
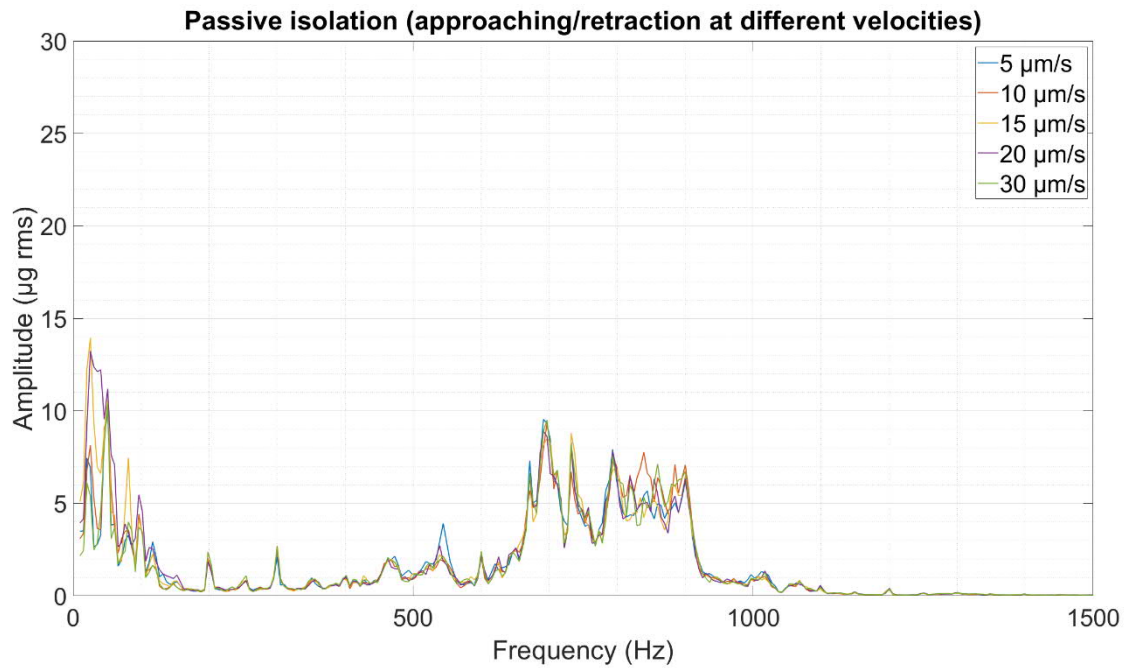
Figure 5.3 Vibration amplitude against different approach and retraction speed when the instrument is installed on a passive vibration isolation table:
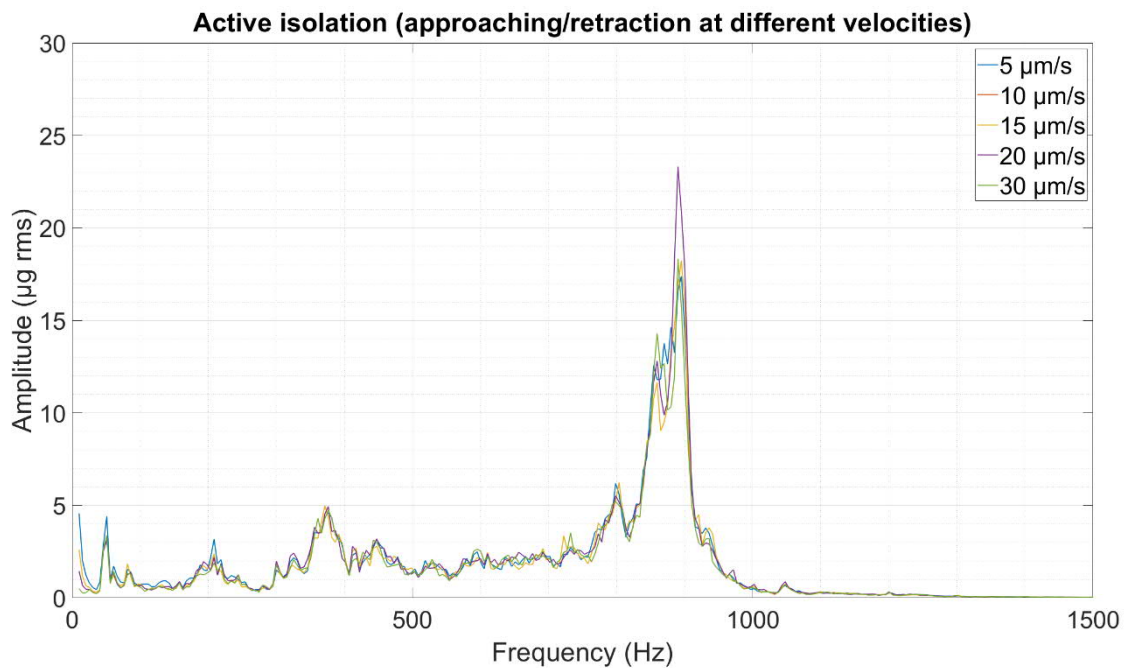Passive vibration isolation table, IsoStation series, Newport company, USA.

Figure 5.4 Vibration amplitude against different approach and retraction speed when the instrument is installed on an active vibration isolation benchtop:
Active vibration isolation benchtop, i4 series, Accurion GmbH, Germany.

Passive or active vibration isolation units are widely used to reduce or ideally cancel internal and external vibrations. Obtained data shows induced vibration for various approach and retraction speed (5-30 $\mu m.s^{-1}$) are not significantly different while the instrument installed on vibration isolation units. The obtained results also confirm active vibration isolation benchtop has a higher performance, especially for low-frequency vibrations.

5.3 Instrument design and reliability

A new SDAM composed of selected modules is designed and implemented. The new instrument also takes advantage of modular design, which facilitates continuous development. New modules can integrate or substitute without significant change in instrument design, previously was hard due to the ad hoc configuration of early-stage SDAM. Implemented adaptive frame provides a high level of flexibility regarding sample format and size. To install asymmetric samples with irregular sizes, the frame can be translated in a horizontal and vertical plane without any change in relative position between stationary modules. Also, the new design offers a higher level of reliability. The movement plane of sample positioning stages is entirely free, and the danger of collision between sample positioning stages and stationery modules is eliminated, as shown in Figure 5.5.
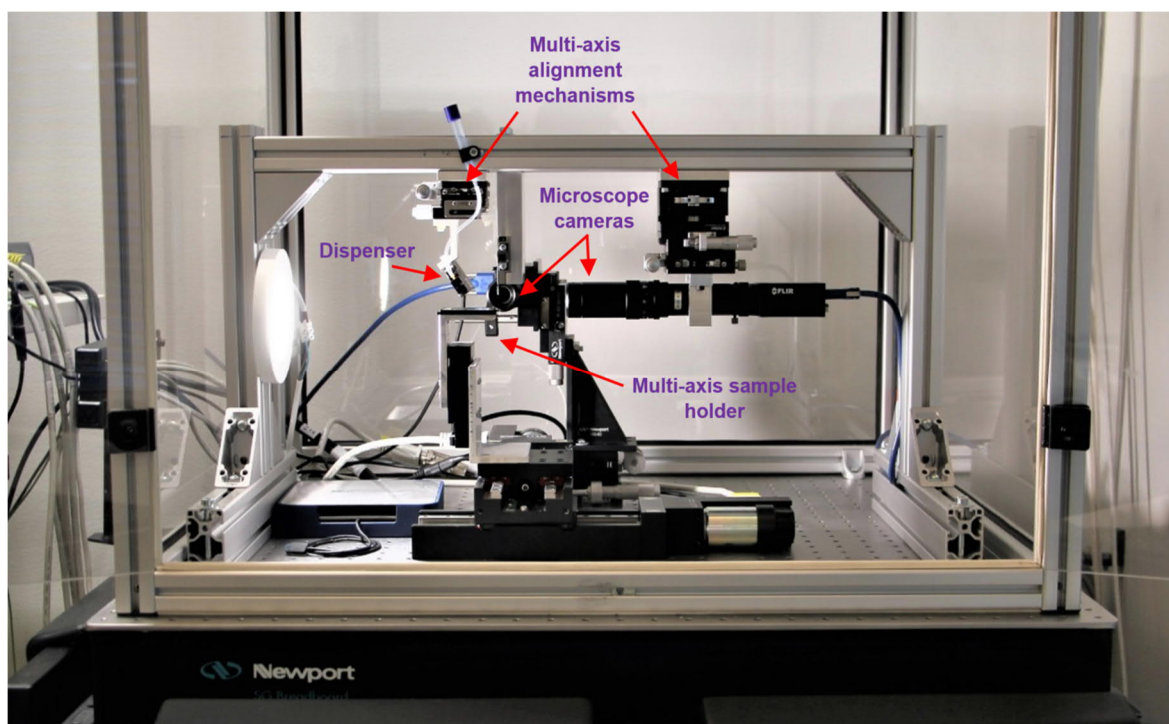

Figure 5.5 New design and implementation for SDAM:
Selected modules for high-performance SDAM are installed in a more compact and efficient configuration.

A summary of quantitative aspects in system performance is given in Table 5.2, to make a comparison between early-stage and new SDAM's key features.

Table 5.2 Summary of tangible improvements in mechatronics design

Property	Early-stage SDAM (unit)	New design SDAM (unit)
preparation time	1-4 (hour)	15-30 (minutes)
Maximum positioning speed in X, Y-axes	20, 50 (mm.s^{-1})	50, 50 (mm.s^{-1})
Maximum positioning speed in Z-axis	3 (mm.s^{-1})	20 (mm.s^{-1})
Workspace	20 × 200 × 5 (mm)	100 × 100 × 25 (mm)
Maximum sample height	5 (mm)	Unlimited
Sample load	10 (N)	50 (N)
Device footprint	750 × 750 (mm)	400 × 600 (mm)

SUMMARY

The scanning droplet adhesion microscopy enables spot-to-spot measurement and 2D wetting maps generation, which can reveal local wetting variations. These regional variations can affect or even govern macroscopic wetting characteristics, which is critical for many applications. Taking advantage of high force sensitivity and spatial resolution in SDAM empowers the surface wetting characterizations in a great deal, especially for superhydrophobic surfaces.

This thesis work introduces SDAM as a robotic instrument for surface wetting characterization. The work is mainly focused on developing a high-performance SDAM, which benefits from a high level of reliability and usability. The role of mechatronics design is providing a robust instrument, which demands systematic instrument design, implementation, and continuous development.

Systematic instrument design for new SDAM is done by the selection and evaluation of reliable modules and components through the iterative process. All modules are evaluated precisely to define individual performance and system interconnections. As a result, the preparation process is sped up from hours down to some minutes. Besides, the instrument has become significantly easier to use by the implementation of new modules, alignment mechanisms, and new system configuration.

The designed instrument complies with the modular design approach to facilitate continuous development. The instrument divides into submodules where each module can be developed without significant change in the instrument architecture. An adaptive platform implemented to support module development. Also, the new design enables customized solutions that is a competitive advantage, especially for a lab instrument.

The new instrument is designed to support high scanning speed and there is no hardware limitation for higher scanning speeds. However, the limiting factors, for instance, the impact of approach and retraction speed on snap-in and pull-off forces, need to be investigated in more detail.

The micro-force sensor is the core technology of SDAM, which suffers from fragility. The new sensor mount is implemented to facilitate sensor installation and eliminate the danger of physical collision. However, issues like uneven quality and short lifetime are significant drawbacks. Finding a substitute technology or developing a customized solution seems necessary.

KOKKUVÕTE

Skaneerimine tilkade haardumine mikroskoopia võimaldab Spot-to-spot mõõtmine ja 2D niisutavate kaartide põlvkonna, mis võib paljastada kohaliku niisutades variatsioone. Need piirkondlikud erinevused võivad mõjutada või isegi reguleerida makroskoopilisi märgtimisomadusi, mis on paljude rakenduste jaoks kriitilise tähtsusega. Suure jõu tundlikkuse ja ruumilise lahutusvõime ärakasutamine SDAM annab suure osa pinna niisutavate iseloomustuse, eriti superhüdrofoobsete pindade puhul.

See väitetöö tutvustab SDAM-i roteerava vahendina pinna niisutamise iseloomustamiseks. Töö keskendub peamiselt suure jõudlusega SDAM-i arendamisele, mis on kõrge usaldusväärsuse ja kasutatavuse tasemega. Mehhatroonika disaini roll on pakkuda tugevat vahendit, mis nõuab süstemaatilist instrumentide kavandamist, rakendamist ja pidevat arengut.

Uue SDAM-i süstemaatilist kavandamist kasutatakse usaldusväärsete moodulite ja komponentide valimisel ja hindamisel iteratiivse protsessi kaudu. Kõiki mooduleid hinnatakse täpselt individuaalsete jõudluse ja süsteemi ühenduste määratlemiseks. Selle tulemusena on ettevalmistusprotsess tundide jooksul kuni mõne minutini välja voolanud. Lisaks on instrument muutunud oluliselt lihtsamaks uute moodulite, vastavusse viimise mehhanismide ja uue süsteemi konfigureerimise abil.

Kavandatud vahend vastab modulaarset disaini lähenemisviisile pideva arengu hõlbustamiseks. Instrument jaguneb alammooduliteks, kus iga moodulit saab arendada ilma instrumendi arhitektuuri olulise muutuseta. Adaptiivne platvorm, mida rakendatakse mooduli arendamise toetamiseks. Samuti võimaldab uus disain kohandatud lahendusi, mis on konkurentsieelis, eriti labori instrumendi jaoks.

Uus instrument on mõeldud toetama kõrge skaneerimise kiirust ja ei ole riistvara piirang kõrgema skaneerimise kiirust. Siiski tuleb üksikasjalikumalt uurida piiravaid tegureid, näiteks lähenemis-ja tagasiheitekiiruse mõju lisandmooduile ja tõmbejõududele.

Mikro-Force sensor on SDAM ' i põhitehnoloogia, mis kannatab ebakindlate jõudude all. Uus andur paigaldada, et hõlbustada sensor paigaldus ja kõrvaldada oht füüsilise kokkupõrge. Kuid probleemid, nagu ebaühtlane kvaliteet ja lühike eluiga, on märkimisväärsed puudused. Asendustehnoloogia leidmine või kohandatud lahenduse väljatöötamine tundub olevat vajalik.

References

[1]   R. Fürstner, W. Barthlott, C. Neinhuis, and P. Walzel, "Wetting and self-cleaning properties of artificial superhydrophobic surfaces," Langmuir, 2005.

[2]   Z. Sun, T. Liao, K. Liu, L. Jiang, J. H. Kim, and S. X. Dou, "Fly-eye inspired superhydrophobic anti-fogging inorganic nanostructures," Small, vol. 10, no. 15, pp. 3001–3006, 2014.

[3]   L. Cao, A. K. Jones, V. K. Sikka, J. Wu, and D. Gao, "Anti-Icing superhydrophobic coatings," Langmuir, 2009.

[4]   Y. Chen, S. Chen, F. Yu, W. Sun, H. Zhu, and Y. Yin, "Fabrication and anti-corrosion property of superhydrophobic hybrid film on copper surface and its formation mechanism," Surf. Interface Anal., vol. 41, no. 11, pp. 872–877, 2009.

[5]   R. N. Wenzel, "Resistance of solid surfaces to wetting by water," Ind. Eng. Chem., vol. 28, no. 8, pp. 988–994, 1936.

[6]   A. B. D. Cassie and S. Baxter, "Wettability of porous surfaces," Trans. Faraday Soc., 1944.

[7]   G. Bracco and B. Holst, Surface science techniques, vol. 51, no. 1. 2013.

[8]   H. Bai, L. Wang, J. Ju, R. Sun, Y. Zheng, and L. Jiang, "Efficient water collection on integrative bioinspired surfaces with star-shaped wettability patterns," Adv. Mater., 2014.

[9]   P. Wang, D. Zhang, and R. Qiu, "Liquid/solid contact mode of super-hydrophobic film in aqueous solution and its effect on corrosion resistance," Corros. Sci., 2012.

[10]   V. Zorba, X. Chen, and S. S. Mao, "Superhydrophilic TiO2 surface without photocatalytic activation," Appl. Phys. Lett., 2010.

[11]   X. Yao, Y. Song, and L. Jiang, "Applications of bio-inspired special wettable surfaces," Advanced Materials. 2011.

[12]   V. Liimatainen et al., "Mapping microscale wetting variations on biological and synthetic water-repellent surfaces," Nat. Commun., vol. 8, no. 1, pp. 1–6, 2017.

[13]   B. Samuel, H. Zhao, and K. Y. Law, "Study of wetting and adhesion interactions between water and various polymer and superhydrophobic surfaces," J. Phys. Chem. C, vol. 115, no. 30, pp. 14852–14861, 2011.

[14]   J. V. I. Timonen, M. Latikka, O. Ikkala, and R. H. A. Ras, "Free-decay and resonant methods for investigating the fundamental limit of superhydrophobicity," Nat. Commun., 2013.

[15]   D. Quéré, "Wetting and Roughness," Annu. Rev. Mater. Res., 2008.

[16]   J. C. Bird, R. Dhiman, H.-M. Kwon, and K. K. Varanasi, "Reducing the contact time of a bouncing drop [Erratum to document cited in CA160:023190]," Nat. (London, U. K.), 2014.

[17] Y. Tian, B. Su, and L. Jiang, "Interfaces: Interfacial Material System Exhibiting Superwettability (Adv. Mater. 40/2014)," Adv. Mater., 2014.

[18] B. Bhushan and Y. C. Jung, "Natural and biomimetic artificial surfaces for superhydrophobicity, self-cleaning, low adhesion, and drag reduction," Progress in Materials Science. 2010.

[19] M. Vuckovac, "Dynamics of Superhydrophobic Surfaces," 2018.

[20] V. Liimatainen, "Control and characterization of wetting at micro- and nanoscale," 2017.

[21] S. Herminghaus, "Roughness-induced non-wetting," Europhys. Lett., 2000.

[22] C. Neinhuis and W. Barthlott, "Characterization and distribution of water-repellent, self-cleaning plant surfaces," Ann. Bot., 1997.

[23] J. W. Drelich, "Contact angles: From past mistakes to new developments through liquid-solid adhesion measurements," Adv. Colloid Interface Sci., vol. 267, pp. 1–14, 2019.

[24] D. Instruments GmbH, "Optical contact angle measuring and contour analysis systems ranging from basic device to fully automated measuring systems for micro-structured samples."

[25] K. L. Mittal, Contact Angle, Wettability and Adhesion, Volume 4. 2018.

[26] K. Y. Law and H. Zhao, Surface wetting: Characterization, contact angle, and fundamentals. 2015.

[27] K. Liu, M. Vuckovac, M. Latikka, and R. H. A. Ras, "Improving surface-wetting characterization," Science (80-.)., vol. 363, no. 6432, pp. 1147–1148, 2019.

[28] H. J. Butt, I. V Roisman, M. Brinkmann, P. Papadopoulos, D. Vollmer, and C. Semprebon, "Characterization of super liquid-repellent surfaces," Curr. Opin. Colloid Interface Sci., vol. 19, no. 4, pp. 343–354, Aug. 2014.

[29] A. Kalantarian, R. David, and A. W. Neumann, "Methodology for high accuracy contact angle measurement," Langmuir, vol. 25, no. 24, pp. 14146–14154, 2009.

[30] S. Srinivasan, G. H. McKinley, and R. E. Cohen, "Assessing the accuracy of contact angle measurements for sessile drops on liquid-repellent surfaces," Langmuir, 2011.

[31] S. Srinivasan, G. H. McKinley, and R. E. Cohen, "Assessing the accuracy of contact angle measurements for sessile drops on liquid-repellent surfaces," Langmuir, vol. 27, no. 22, pp. 13582–13589, 2011.

[32] "Sigma 700/701, Force Tensiometers." [Online]. Available: https://www.biolinscientific.com/attension/force-tensiometers/sigma-700-701. [Accessed: 19-Dec-2019].

[33] J. A. Kleingartner, S. Srinivasan, J. M. Mabry, R. E. Cohen, and G. H. McKinley, "Utilizing dynamic tensiometry to quantify contact angle hysteresis and wetting

state transitions on nonwetting surfaces," Langmuir, 2013.

[34] B. Samuel, H. Zhao, and K. Y. Law, "Study of wetting and adhesion interactions between water and various polymer and superhydrophobic surfaces," J. Phys. Chem. C, 2011.

[35] M. Liu, S. Wang, Z. Wei, Y. Song, and L. Jiang, "Bioinspired design of a superoleophobic and low adhesive water/solid interface," Adv. Mater., vol. 21, no. 6, pp. 665–669, 2009.

[36] Y. Lai, X. Gao, H. Zhuang, J. Huang, C. Lin, and L. Jiang, "Designing superhydrophobic porous nanostructures with tunable water adhesion," Adv. Mater., vol. 21, no. 37, pp. 3799–3803, 2009.

[37] M. Delmas, M. Monthioux, and T. Ondarçuhu, "Contact angle hysteresis at the nanometer scale," Phys. Rev. Lett., vol. 106, no. 13, pp. 1–4, 2011.

[38] K. Latifi, "Seyed Kourosh Latifi Measurement of Z-Directional Individual Fibre-Fibre Bond Strength and Microfibril Angle Using," 2014.

[39] S. Fahlbusch and S. Fatikow, "Force sensing in microrobotic systems - an overview," Proc. IEEE Int. Conf. Electron. Circuits, Syst., vol. 3, pp. 259–262, 1998.

[40] Y. Sun, S. N. Fry, D. P. Potasek, D. J. Bell, and B. J. Nelson, "Characterizing fruit fly flight behavior using a micro-force sensor with a new comb-drive configuration," J. Microelectromechanical Syst., vol. 14, no. 1, pp. 4–11, 2005.

[41] M. Haris and H. Qu, "A CMOS-MEMS nano-newton force sensor for biomedical applications," 2010 IEEE 5th Int. Conf. Nano/Micro Eng. Mol. Syst. NEMS 2010, pp. 177–181, 2010.

[42] M. Bulut Coskun, S. Moore, S. O. R. Moheimani, A. Neild, and T. Alan, "Zero displacement microelectromechanical force sensor using feedback control," Appl. Phys. Lett., vol. 104, no. 15, 2014.

[43] M. Maroufi, H. Alemansour, M. Bulut Coskun, and S. O. Reza Moheimani, "An adjustable-stiffness MEMS force sensor: Design, characterization, and control," Mechatronics, vol. 56, no. March, pp. 198–210, 2018.

[44] N. Blanc, "Scanning force microscopy in the dynamic mode using microfabricated capacitive sensors," J. Vac. Sci. Technol. B Microelectron. Nanom. Struct., 1996.

[45] "Micro-force Sensing Probe, Femto Tools." [Online]. Available: https://www.femtotools.com/previousproducts/ft-s-microforce-sensing-probe. [Accessed: 23-Jul-2019].

[46] "Microdispenser, GeSiM." [Online]. Available: https://gesim-bioinstruments-microfluidics.com/dispensers-and-accessories/. [Accessed: 23-Jul-2019].

[47] A. Kossiakoff, W. N. Sweet, S. J. Seymour, and S. M. Biemer, Systems Engineering Principles and Practice: Second Edition. 2011.

[48] R. Sell and M. Tamre, "Integration of V-model and SysML for advanced mechatronics system design," Proc. Res. Educ. Mechatronics Conf. REM05, pp. 276–280, 2005.

[49] "PipeJet Microdispenser, BioFluidix." [Online]. Available: http://www.biofluidix.com/products/single-channel-dispensers/pipejet.html. [Accessed: 23-Jul-2019].

[50] "VZM^{TM} 600i Zoom Imaging Lens, Edmund Optics." [Online]. Available: https://www.edmundoptics.com/p/vzmtrade-600i-zoom-imaging-lens-3164102e/30657/. [Accessed: 23-Jul-2019].

[51] "Pixel Sizes and Optics, Edmund Optics." [Online]. Available: https://www.edmundoptics.com/knowledge-center/application-notes/imaging/pixel-sizes-and-optics. [Accessed: 19-Dec-2019].

[52] "Object Space Resolution, Edmund Optics." [Online]. Available: https://www.edmundoptics.com/knowledge-center/application-notes/imaging/object-space-resolution/. [Accessed: 19-Dec-2019].

To study the impact of approach and retraction speed, 100 spots on a fluoropolymer coated black silicon measured. Obtained snap-in and pull-off forces are plotted versus approach and retraction speed for all measurement points, shown in Figure A. The obtained results reveal snap-in force grows when approach speed is increasing while the pull-off force is much less sensitive to retraction speed. According to the obtained snap-in and pull-off forces, 5 µm.s^{-1} has chosen as an optimum velocity for approach and retraction.
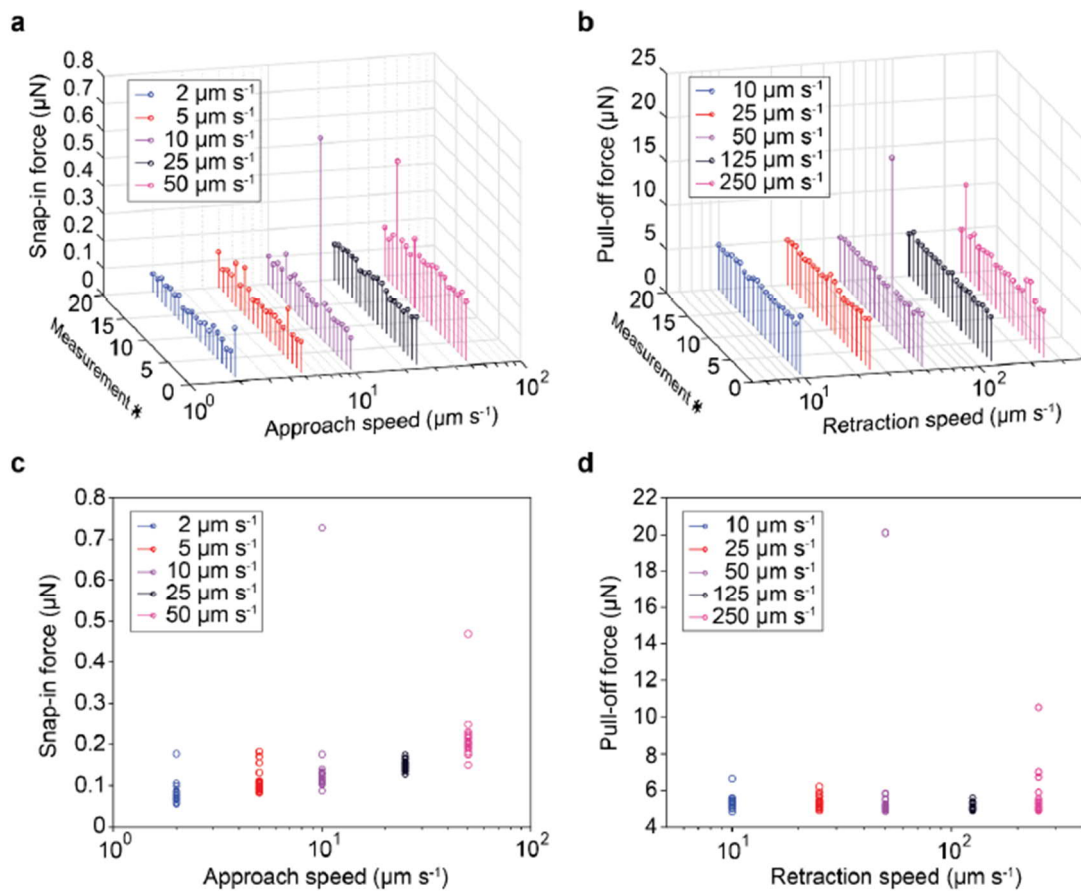
Figure A. Droplet adhesion forces versus different approach/retraction speed:
(a) Snap-in force versus five different approach speed and (b) pull-off force versus retraction speed for 100 different spots on a fluoropolymer coated black silicon with the corresponding (c,d) 2D projections [12].